MEAN LANDSLIDE GEOMETRIES INFERRED FROM A GLOBAL DATABASE OF EARTHQUAKE- AND NON-EARTHQUAKE-TRIGGERED LANDSLIDES

Gisela DOMEJ[(*)(**)], Celine BOURDEAU[(**)], Luca LENTI[(*)],
Salvatore MARTINO[(***)] & Kacper PLUTA[(****)]

[(*)]*IFSTTAR - GERS - Séismes et Vibrations - 14-20 Boulevard Newton - Cité Descartes - 77447 Marne-la-Vallée, France*
[(**)]*IFSTTAR - GERS - Sols, Roches et Ouvrages Géotechniques - 14-20 Boulevard Newton - Cité Descartes - 77447 Marne-la-Vallée, France*
[(***)]*Sapienza Università di Roma - CERI e Dipartimento di Scienze della Terra - Piazzale Aldo Moro, 5 - 00185 Rome, Italy*
[(****)]*Université Paris-Est LIGM & LAMA - 6-8 Avenue Blaise Pascal - Cité Descartes - 77455 Marne-la-Vallée, France*
Corresponding author: gisela.domej@ifsttar.fr

EXTENDED ABSTRACT

Le frane sono processi innescati da differenti azioni: piogge, terremoti, interventi antropici ed esplosioni. A seconda dell'intensità di tali azioni, gli effetti delle frane possono essere trascurabili o disastrosi causando vittime ed ingenti danni alle attività antropiche e all'ambiente.

A tale riguardo, l'azione sismica è particolarmente interessante dato che la conformazione del rilievo con una eventuale massa di frana presente possono modulare le onde sismiche.

Uno degli esempi più disastrosi di frane sismoindotte è rappresentato dall'evento di Nevado Huascarán, una *rock avalanche* innescata dal sisma del Perù del 31/05/1970 che ha seppellito le città di Yungai e Ranrahirca causando 54.000 morti. In Italia, nel corso della sequenza sismica del 1783, una *rock avalanche* si innesco' in adiacenza alla costa tirrenica vicino l'abitato di Scilla causando circa 1.500 vittime per effetto dello tsunami generato dall'impatto della massa rocciosa in mare.

La ricerca sugli effetti di sito e la loro relazione con l'innesco di frane è da tempo condotta attraverso differenti metodi di analisi di stabilità. La maggior parte di questi è limitata ad ipotesi 2D dal momento che più complessi approcci 3D necessitano a tutt'oggi di ulteriori validazioni. Le ipotesi 3D, d'altro canto, considerano meglio le condizioni al contorno esistenti ai bordi della massa di frana, importanti per valutare l'intrappolamneto delle onde sismiche.

Nel tempo, diversi dati sono stati inventariati per stabilire possibili relazioni tra le frane sismoindotte e la loro distribuzione spaziale. In questo studio sono stati censiti 277 frane a scala globale, delle quali un terzo riferito a frane storicamente sismoindotte, per dedurre mediante un approccio statistico parametri geometrici caratteristici di frane 3D. La classificazione degli eventi adottata segue gli standard internazionali condivisi dalla comunità scientifica.

In una prima fase, i dati archiviati sono stati confrontati mediante relazioni empiriche di letteratura mettendo in luce un buon accordo con quanto dedotto da precedenti autori ed è stata validata la completezza dell'archivio considerato.

Da questa analisi è risultato che caratteristiche geometriche connesse alla rappresentazione in pianta ed alla restituzione lungo sezioni longitudinali delle frane sono più riportate in letteratura rispetto a quelle legate alle sezioni trasversali che, al contrario, sono raramente presenti negli studi o nei rapporti tecnici. Questa carenza di informazioni se da un lato non pesa sulle ricostruzioni 2D e sulle relative modellazioni numeriche, dall'altro limita la definizione dei corpi 3D per ciò che attiene la delimitazione laterale delle masse stessa. In base all'archivio ricostruito, le informazioni geometriche inerenti le masse di frana risultano complete al 50-70% solo per i due terzi delle frane.

Dapprima è stata analizzata la distribuzione statistica dei parametri dedotti dai dati di archivio, ottenendo distribuzioni di frequenza di parametri, organizzati in 3 gruppi tipologici e dimensionati su 30 classi; sono state, quindi, cercate le distribuzioni statistiche, normali o leggi di potenza, che meglio approssimassero le suddette distribuzioni. Dall'analisi complessiva di tutti i parametri è risultato che le distribuzioni di frequenza relative ai parametri relazionati alla dimensione hanno un decremento esponenziale mentre quelle relative ai parametri relazionati alla forma sono di tipo normale. Sono state, dunque, selezionate 3 classi dimensionali riferite a volumi di 10^3-10^6 m³, 10^6-10^9 m³ and 10^9-10^{12} m³ ed ottenute 9 serie di dati, dai 3 gruppi tipologici di parametri, a loro volta distinti per le 3 classi dimensionali. In base al confronto dei valori medi riferiti ai parametri geometrici atti a rappresentare condizioni 1D, 2D e 3D è emerso che essi aumentano con la classe dimensionale mentre la media dei valori angolari, dei rapporti di forma e delle curvature resta all'incirca costante.

Da questo studio affermiamo che: a) i parametri dimensionali e quelli di forma non aumentano con la stessa legge all'aumentare della classe dimensionale della frana; b) i parametri di forma non sono influenzati dal contenuto nell'archivio; c) i parametri di forma sono poco influenzati dalla classe dimensionale.

Questi risultati sono rivelanti per la progettazione di modelli numerici finalizzati al calcolo degli spostamenti sismoindotti dato che in letteratura è già dimostrato che forma della frana e posizione relativa del bedrock incassante influiscono sulle interazioni tra onde sismiche e versanti avendo effetto sulla risposta sismica locale e sulla mobilità.

ABSTRACT

Ranging in size from very small to tremendous, landslides often cause loss of life and damage to infrastructure, property and the environment. They are triggered by a variety and combinations of causes among which the role of water and seismic shaking have the most serious consequences. In this regard, seismic wave amplification due to topography as well as to the impedance contrast between the landslide mass and its underlying bedrock are of particular interest. Therefore, high resolution reconstruction of the lateral confinement of the landslide mass and the exact measurement of the mechanical properties are a necessity.

A global chronological database was created to study and compare 2D and 3D geometries of landslides, i.e. of landslides properly sliding on a rupture surface. It contains 277 seismically and non-seismically induced landslides whose rupture masses were measured in all available details allowing for statistical analyses of their shapes and to create numerical models thereupon based.

Detailed studies reveal that values of distinct geometrical parameters have different statistical behaviors. As for dimension related parameters, occurrence frequencies follow decreasing exponential distributions and mean values progressively increase with landslide magnitude. In contrast, occurrence frequencies of shape-related parameters follow normal distributions and mean values are constant throughout different landslide magnitudes. Dimensions and shapes of landslides are thus to be regarded in a precise and distinctive manner when analyzing seismically induced slope displacements.

INTRODUCTION

Landslides are worldwide common phenomena triggered by a variety of causes such as heavy precipitation, strong storms, natural seismic activity, artificial load changes, clay involvement, or even blasts. Often causes interfere with each other and combined triggers are not scarce. On a global scale, the role of water, seismic and volcanic activity seem to have the most relevant effects (USGS, 2004). Depending on the size of an event, consequences can be minor to disastrous causing loss of life and considerable damage to infrastructure, property and the environment (BIRD & BOMMER, 2004). One main reason for more frequent catastrophes is the growth of population which entails extending urbanization to areas with high landslide potential.

Throughout literature, reports and case studies on seismically induced mass movements as well as site effects are abundant. In terms of fatalities the most disastrous example might be the rock avalanche at Nevado Huascarán, Peru, which was triggered by the Peruvian Earthquake (or Ancash Earthquake; M_W=7.9) on 31st of May 1970 and buried the towns of Yungai and Ranrahirca causing

54,000 victims (KUROIWA *et alii*, 1970; LOMNITZ, 1970). Also three more recent mass movement events drew a line of catastrophic destruction and a high rate of loss of life. The El Salvador Earthquake on 13th of January 2001 (M_W=7.6) triggered several landslides in Santa Tecla and Comasagua killing 500 people (EVANS & BENT, 2004). During the Hattian Bala rock avalanche triggered by the Kashmir Earthquake (M_W=7.6) on 8th of October 2005 around 25,000 residents of the Jhelum Valley, Pakistan, lost their lives (DUNNING *et alii*, 2007). An equally high number of victims (20,000) amounts from the landslide series in and around Beichuan, China, after the Sichuan Earthquake (or Wenchuan Earthquake; M_W=7.9) on 12th of May 2008 (YIN *et alii*, 2009). In contrast to such deadly events, there are also mass movements that initially claim a rather low number of fatalities but pose a long term secondary threat to the environment and the local population. For instance, the Sarez Earthquake of 18th of February 1911 (M_W=7.2) triggered a gigantic landslide that finally blocked the Murghab River, Tajikistan, creating a natural dam. This dam appears to be the world's largest natural dam and it permanently poses the threat of a leakage or deluge (PREOBRAZHENSKY, 1920; SCHUSTER & ALFORD, 2004; AMBRASEYS & BILHAM, 2012). Multihazard chain effects are also documented in historic chronicles. The Calabria Earthquake on 6th of February 1783 (M_W=6.2) is reported to have triggered the Scilla Landslide that slid into the sea. The hereby induced tsunami wave caused 1500 casualties at a nearby coastline agglomeration (BOZZANO *et alii*, 2011).

Over time, the long-living assumption of mass movements being simply secondary effects of earthquakes was revised and the topic became a focus of interest. Seismic shaking is of particular importance since convex topographies as well as a landslide mass itself can trap waves and hence amplify incoming body waves – a phenomenon known as site effects. Today, research on site effects and seismically induced landslides is extensive and a broad spectrum of methods for modeling slope deformation is available. Those methods range from pseudo-static and rigid-block-based methods to numerical models. The majority is limited to 2D modeling since more sophisticated approaches in 3D are still under development or need calibration. However, the effect of lateral confinement in 3D is of great importance because it may enhance the focusing of trapped waves in the landslide mass contributing to the landslide reactivation under seismic shaking.

To establish correlations between mass movement features and the characteristics of their causes scientists established databases. The first and most cited of its kind is a set of 40 earthquake-triggered landslides presented by KEEFER in 1984. He empirically related magnitudes of earthquakes to the maximum distance at which the respective mass movements occurred; similarly, he also correlated area affected by mass movement events to the respective magnitude of the earthquake. In 1999 RODRÍGUEZ *et alii* published an extension of this work. Other

studies associate landslide volumes with moment magnitudes M_w and seismic moments M_0 (Keefer, 1994; Martino *et alii*, 2014) or with the affected area (Guzzetti *et alii*, 2009). In contrast to global catalogues, event-based databases often try to relate landslide volumes to a variety of parameters. For instance, Xu *et alii* (2016) estimate the total volume of all landslides triggered by the Sichuan Earthquake by evaluating six distinct landslide parameters and the peak ground acceleration.

Sharing the aim of data creation for comparative statistical analyses and numerical modeling of earthquake-triggered landslides to shed light on the causes of such events a new global landslide database was built. This paper presents in the first part the database itself; properties, the way of construction, advantages and some drawbacks will be discussed. The second part shows the statistical analyses that were carried out using the database and it presents nine mean landslide geometries inferred from the database.

These simplified landslide geometries will be useful for later studies to predict slope stability considering mechanical and geometrical properties as well as the properties of the potential seismic impact. The contributions of trapped seismic waves to the displacement of the landslide mass can then be numerically modeled by different approaches in 2D and 3D.

CONSTRUCTION AND PROPERTIES OF THE DATABASE

Usually two types of databases for mass movements are to be distinguished – event-based and chronological databases. The first type ideally represents a complete inventory of mass movements after a certain triggering event such as intense rainfall, severe storms (like hurricanes and typhoons) or earthquakes. The second type inventorizes mass movements characterized by more than one trigger chronologically according to their occurrences. For both types completeness is a crucial factor because statistical analyses of event-based databases in particular might lead to false conclusions when dealing with incomplete or inaccurately assessed datasets (Malamud *et alii*, 2004).

The database presented in this article is of chronological nature and also does not claim completeness. It contains a set of globally distributed mass movements with different triggers of which a third are earthquakes. It should be noted that the term "landslide" is wide-spread throughout literature designing rock falls, rock avalanches, debris flows, toppling and different types of slope failure. The more general term "mass movement" also includes soil settlements and liquefaction. This database focuses on proper "sliding" mechanisms according to the classification of Varnes (1978). Unfortunately, because of different scientific viewpoints and gradual transitions between mass movement types (Fig. 1), landslide classification is not always trivial and hence might be misleading as it will be discussed in the following.
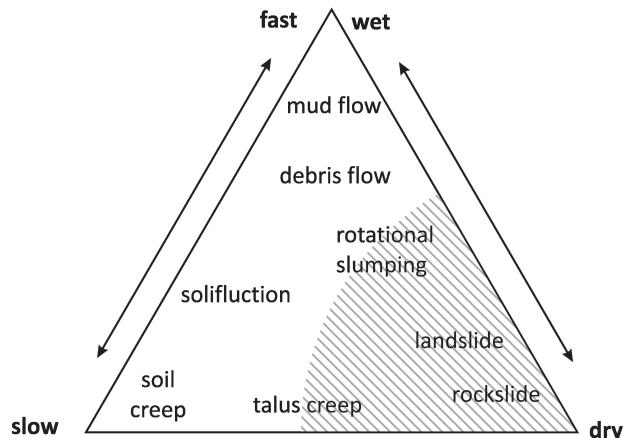

Fig. 1 - *Mass movement triangle (after Carson & Kirkby, 1972). The focus of the here presented database is on the shaded area referring to proper sliding mechanisms*

For the construction of the database documented landslide cases in the available literature were evaluated as suitable or the opposite when coming across them in no particular order and without pre-selection. At the present stage the database contains 277 landslides in 40 countries (Appendix I; Tab. 1) – a sufficient number for relevant statistical analyses.

The main concept of data collection followed suggestions by the International Geotechnical Societies' Unesco Working Party on World Landslide Inventory (1990, 1991, 1993, 1994) and the International Union of Geological Sciences Working Group on Landslides (1995) that indicate how to establish landslide reports and summaries and how the activity, the rate of movement and the causes of a landslides should be described. Based on these suggestions a "survey chart" with many more landslide characteristics was developed. A blank survey chart is presented in the Appendix II.

The first section on the front page is dedicated to the identification of a landslide listing basic information such as name,

COUNTRY	EACH
Italy	50
Canada	29
Belgium	27
China, USA	22
Chile, Spain	10
Switzerland	8
France, Kyrgyzstan	7
Algeria, Japan, New Zealand, Tajikistan, Turkey, Ukraine	6
Austria, Norway, Taiwan	5
Czech Republic, Slovakia	4
Iran, Peru	3
Australia, Croatia, Poland	2
Armenia, Barbados, Bhutan, Cape Verde, Ecuador, El Salvador, Germany, Liechtenstein, Mongolia, Pakistan, Panama, Russia, Slovenia, United Kingdom	1
TOTAL	**277**

Tab. 1 - *Landslide distribution per modern-day country displaying also the availability of landslide data in different regions*

its number in the database, precise location and sliding direction, date, fatalities and damage if reported and the relation to a seismic trigger. In contrast to the detailed activity phases described by the INTERNATIONAL GEOTECHNICAL SOCIETIES' UNESCO WORKING PARTY ON WORLD LANDSLIDE INVENTORY (1993), the database presented in this article distinguishes only between active/slow, active/fast (both together 153 cases; 55%) and inactive (124 cases, 45%) landslides. The subsection of involved material is based on the classification of VARNES (1978) appointing rock, soil and/or debris as the three materials of which a landslide mass may be composed. Locations are given with respect to geographical references and as coordinate points. 220 landslides (79%) are located in currently seismic areas across the globe, 50 landslides (18%) are to be found in rather less or non-seismic areas and 7 landslides (8%) are situated in areas that used to be seismically active but came to tectonic stability.

Second, the section of landslide imagery gives information on how well literature documents a landslide visually – i.e. if publications show a map, a longitudinal cross section (LCS), a three-dimensional model and/or photographs. An interesting finding becomes apparent though graphical representation of the availability of landslide imagery (Fig. 2). By far not for all landslides literature offers maps and LCS even though both of them are of great importance for the characterization of a landslide. For instance, only 216 cases (80%) have a map, for 202 cases (71%) an LCS is available and only 168 landslides (61%) are described by both a map and an LCS. Considering that the selection of cases and respective literature did not follow any preference, this leaves the general question about the average level of completeness of publications.

The third section refers to landslide causes and indicates the triggers of a landslide or their combinations. Of the 277 landslides 99 (36%) have or may have been seismically induced; the uncertainty is explained by the fact that – compared to recent seismically induced landslides with a well documented time history – for certain paleo-landslides a seismic trigger can
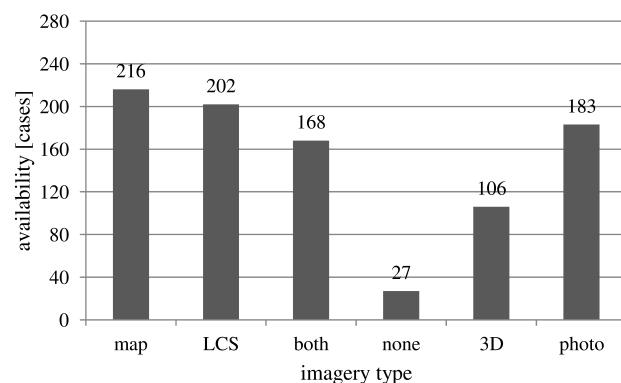
only be assumed but not confirmed. Of those 99 landslides 74 (75%) definitely have a seismic cause. 85 landslides (86%) are co-seismic, 11 landslides (11%) are post-seismic, and in the remaining 3 cases (3%) the main rupture process over a longer period of time. It should be mentioned that the database considers earthquakes, blasts (5 cases) and repeated strong volcanic activity (2 cases) as seismic activity.

Finally, the fourth section lists all publications from which information was retrieved and introduced to the survey chart satisfying the suggestion of the INTERNATIONAL GEOTECHNICAL SOCIETIES' UNESCO WORKING PARTY ON WORLD LANDSLIDE INVENTORY (1990) that references must remain traceable.

The back side of the survey chart is dedicated to the geometry of a particular landslide. Based on the suggested nomenclature for landslides proposed by the COMMISSION ON LANDSLIDES OF THE INTERNATIONAL ASSOCIATION OF ENGINEERING GEOLOGY (1990) a much more detailed set of parameters was elaborated which reports ideally – if literature is exhaustive enough – 66 single parameters and descriptive notes (Fig. 3; Tab. 2) all referring to the rupture mass of a landslide, i.e. either the landslide mass confined by the rupture surface at the instance of the major sliding event, or the total moving mass in case of active landslides.

The geometry section of the survey chart is separated into seven sections describing principal geometry, volume, area, LCS, map, transversal cross sections I-III (TCS I-III) and ratios. It also displays a small figure of the LCS according to the inserted respective values that served as a verification tool during the process of data assessment.

Distinction is made between rotational, translational and roto-translational landslides. This distinction becomes useful when calculating volumes of landslides. The volume of a landslide is an important parameter controlling its impact but it is also the most difficult to assess. In contrast to many landslide databases that report deposit volumes, for the database presented in this article only rupture volumes are of interest. According to CRUDEN & VARNES (1996) they can be approximated by calculating the volume of half an ellipsoid (Eq. 1). However, this equation fits best for perfectly rotational landslides with very flat original surface topographies. The more the rupture geometry deviates from this perfect half ellipsoid the more the equation overestimates the volume and for translational and roto-translational landslides it might not deliver trustable results.

$$V = (1/6) \, \pi \, L \, D \, W \qquad \text{(Eq. 1)}$$

The volume section offers two cells: one cites the volume reported in literature, the other calculates the volume according to the equation proposed by CRUDEN & VARNES (1996).

Similarly, the section storing the area A of a landslide refers to the landslide area measured on the original topography before the sliding event. The horizontal projection A_h differs from A by the factor of the cosine of the mean slope angle α.


Fig. 2 - Availability of landslide imagery in literature with respective numbers of cases (from left to right: map only, LCS only, map and LCS, neither map nor LCS, 3D representation, photography)
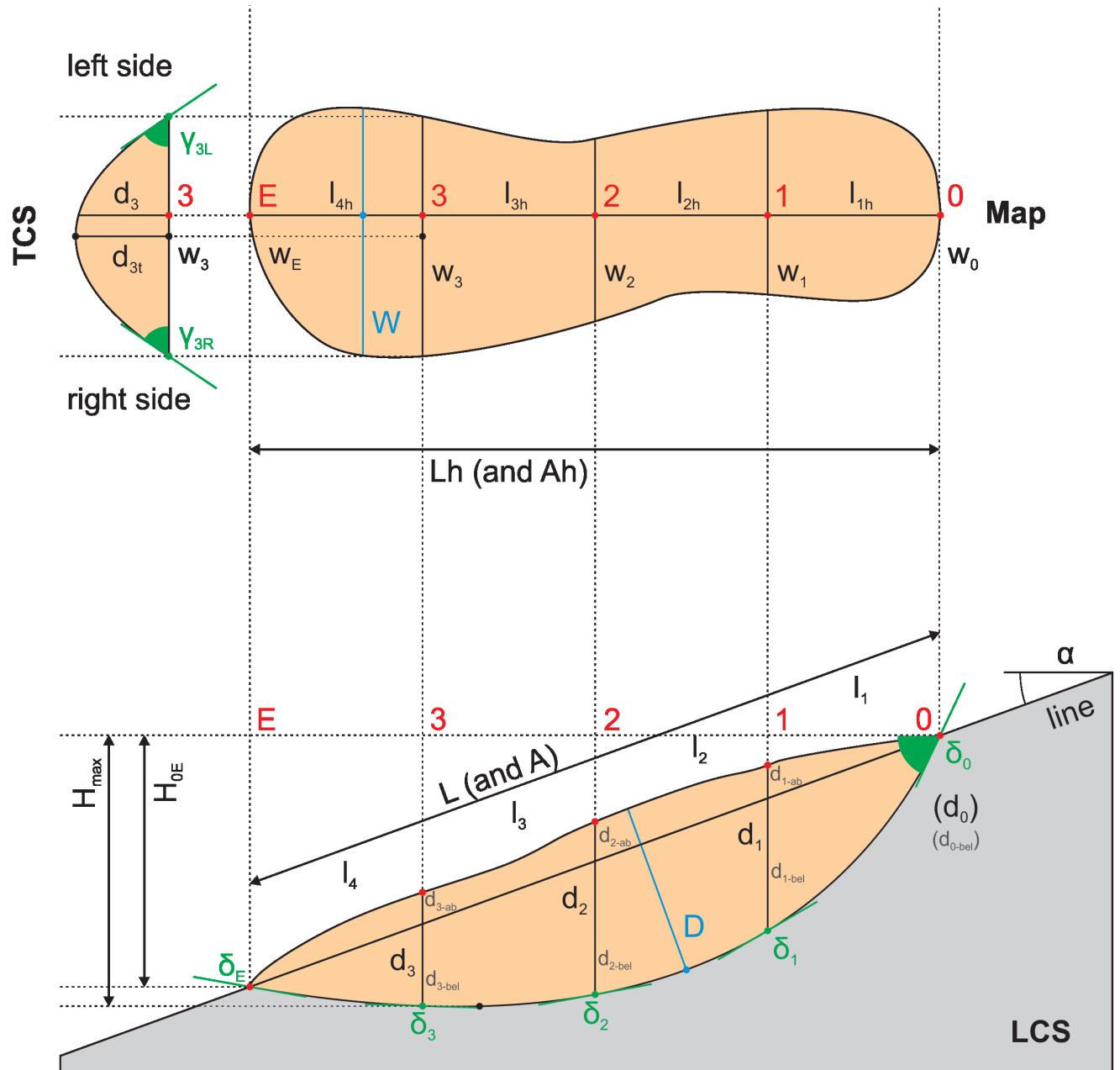
Fig. 3 - Illustration of landslide geometry parameters in a plane view (map) and 2D cross sections (LCS & TCS). Abbreviations are described in Tab. 2. In contrast to the definition of "left and right" by the COMMISSION ON LANDSLIDES OF THE INTERNATIONAL ASSOCIATION OF ENGINEERING GEOLOGY (1990), the two sides are here defined by looking upwards to the landslide crest (i.e. from point E to point 0). The straight connection of the first main geometry point (0) and the last one (E) is simply entitled the "line"; with respect to the horizontal it defines the mean slope angle α. The two parameters d_0 and d_{0-bel} are noted in brackets because they may or may not exist at a specific landslide since not every landslide mass detaches with a trench below point 0

The section of the LCS is the most extensive and meaningful reporting lengths, depths, heights and angles along the average sliding surface with respect to the five main reference points 0, 1, 2, 3 and E (for "end"). Angles δ are measured between a tangent plane to the sliding surface and the horizontal in the direction of sliding; negative angles are possible when the sliding surface curves up (Fig. 3).

The map section displays values measured from the horizontal projection of a landslide and the section of TCS I-III gives information on the lateral dimensions of a landslide. Ideally

there would be three clear TCS for every landslide indicating depths (d_{1t}, d_{2t} and d_{3t}) as well as the respective flank angles (γ_{1L}, γ_{1R}, γ_{2L}, γ_{2R}, γ_{3L} and γ_{3R}) to design a 3D enveloping confinement. Unfortunately TCS appear very seldom in literature and lateral shapes can only be assumed. For such assumptions the TCS section offers four cells where one of the following four shapes

per TSC position can be chosen: "V" for V-shape, "(" for a flat concave shape, "[" for a drawer-like shape and "U" for a U-shape. Despite its great importance for assessing the behavior of a landslide mass under seismic shaking in 3D through numerical modeling this section is of less use since only 2 of 277 cases allow for complete TCS characterization.

PARAMETER	EQUATION / NOTE	DESCRIPTION
principal geometry	rot, trans or rotrotrans	principal geometry type
V_{lit}		volume as by literature
V_{equ}	$= (1/6)*\pi*L*D*W$	volumes as by equation
A		area
A_h	$= A*\cos(\alpha_{equ})$	area projected to horizontal
L	$= L_h/\cos(\alpha_{equ})$	length
L_h		length projected to horizontal
$l_1 = l_2 = l_3 = l_4$	$= L/4$	length parts
$l_{1h} = l_{2h} = l_{3h} = l_{4h}$	$= L_h/4$	length parts projected to horizontal
H_{max}		height between point 0 and deepest point
H_{0E}		height between point 0 and point E
W		maximum width
w_0		width at point 0
w_1		width at point 1
w_2		width at point 2
w_3		width at point 3
w_E		width at point E
w_{av}	$= (w_0+w_1+w_2+w_3+w_E)/5$	average width
D		maximum depth
d_0		depth at point 0 (if existing)
d_1		depth at point 1
d_2		depth at point 2
d_3		depth at point 3
d_E	always 0	depth at point E
d_{av}	$= (d_0+d_1+d_2+d_3+d_E)/5$	average depth
d_{0-ab}	always 0	depth part at point 0 (above line)
d_{1-ab}		depth part at point 1 (above line)
d_{2-ab}		depth part at point 2 (above line)
d_{3-ab}		depth part at point 3 (above line)
d_{E-ab}	always 0	depth part at point E (above line)
d_{0-bel}	$= d_0-d_{0-ab}$	depth part at point 0 (below line, if existing)
d_{1-bel}	$= d_1-d_{1-ab}$	depth part at point 1 (below line)
d_{2-bel}	$= d_2-d_{2-ab}$	depth part at point 2 (below line)
d_{3-bel}	$= d_3-d_{3-ab}$	depth part at point 3 (below line)
d_{E-bel}	$= d_E-d_{E-ab}$ = always 0	depth part at point E (below line)
δ_0		rupture surface inclination at point 0
δ_1		rupture surface inclination at point 1
δ_2		rupture surface inclination at point 2
δ_3		rupture surface inclination at point 3
δ_E		rupture surface inclination at point E
α_{lit} (literature)		mean slope angle as by literature
α_{equ} (equation)	$= \tan^{-1}(H_{0E}/L_h)$	mean slope angle as by equation
D/L (ratio)	$= D/L$	ratio "maximum depth / length"
w_{av}/L_h (ratio)	$= w_{av}/L_h$	ratio "average width / projected length"
H_{max}/L_h (ratio)	$= H_{max}/L_h$	ratio "maximum height / projected length"
d_{1t}, d_{2t}, d_{3t}		maximum depths of TCS I, II and III
γ_{1L}, γ_{2L}, γ_{3L}		left flank angles of TCS I, II and III
γ_{1R}, γ_{2R}, γ_{3R}		right flank angles of TCS I, II and III
rough width shape	to tick either V, (, [or U	rough width shapes of TCS I, II and III

Tab. 2 - Full list of landslide geometry parameters. It should be noted that the survey chart cell of the principal geometry does not contain values but one out of three options to choose; for the rough width shapes one of four survey chart cells can be chosen. By definition, the content of the survey chart cells d_E, d_{0-ab}, d_{E-ab}, d_{E-bel} are always 0. The "0" in the equation column and at indices of parameters is not to be confounded; one is a defined value, the other refers to the first of the five main geometry positions (Fig. 3)

The three proportions (D/L, w_{av}/L_h and H_{max}/L_h) shown in the ratio sections serve for quick comparison of landslides. As analyses will show later, it seems though more suitable to use the rather uniform ratios d_{av}/L, w_{av}/L_h, d_{av}/w_{av} and H_{0E}/L_h as well as curvature values of landslides to compare their shapes.

To enable efficient and accurate data analyses, the complete content of the survey charts is stored in a Microsoft Access database. It allows for fast filtering and sorting to create data for statistical analyses.

STATISTICAL EXPLORATION OF THE DATABASE
Magnitude-distance-relations comparing to Keefer's curve

Based on a set of 40 seismically induced landslides KEEFER (1984) related magnitudes of earthquakes to the maximum distances at which mass movements occurred. Distances relations are shown with respect to the epicenter and to the fault rupture zone locations separately. KEEFER (1984) distinguished disrupted falls and slides, coherent slides and lateral spreads and flows. To compare the data presented in this article to the proposed curves by KEEFER (1984) only the one of coherent slides was chosen as reference since it fits best the definition of landslides included in the here presented database.

In total the database contains 99 seismically induced landslides of which 72 are proven to have an earthquake as trigger. For all of them either moment magnitudes (M_W) or surface wave magnitudes (M_S) were retrieved from the bulletin of the INTERNATIONAL SEISMOLOGICAL CENTER (2016) and the EUROPEAN ARCHIVE OF HISTORICAL EARTHQUAKE DATA (2016). Indeed, it is not ideal to represent two types of magnitudes in the same graph, but since M_S saturates at higher values, big earthquakes are rather to be covered by using M_W. Also KEEFER (1984) used both magnitude types in his graphs. As a result, 62 landslides were triggered by an earthquake reported in M_W, 8 landslides were triggered by an earthquake reported in M_S and the remaining 2 landslides were triggered by an earthquake with unknown magnitude type (M_{ukn}; Fig. 4).

Because there is no available information about the exact fault rupture location or the hypocenter for the 22 historical earthquakes among the set of 72, comparative magnitude-distance relations are limited to epicenter distances. Values refer to the length of the connecting line between the official epicenter and the landslide along the Earth's surface with respect to the World Geodetic System 1984 (WGS 84). It should be noted that epicenter-landslide distances might vary significantly from hypocenter-distances especially if the hypocenter is deep.

However, only 2 of the 72 concerned earthquakes appear to be deep (El Salvador Earthquake on 13th of January 2001, M_W=7.6, 82.9 km; Sanriku-Minami Earthquake on 26th of May 2003, M_W=7.0, 71.2 km) whereas all other cases do not exceed the Mohorovičić discontinuity.

In agreement to results of DELGADO *et alii* (2011), the scatter is big and some points reach the reference curve or even exceed it. Reasons might be topographic and/or lithological site effects, precipitation events and soil weakening earthquake swarms. Interestingly, two of the three points that lie highly above the curve are likewise described as outliers by DELGADO *et alii* (2011; Tab. 3) and all three have an offshore epicenter.
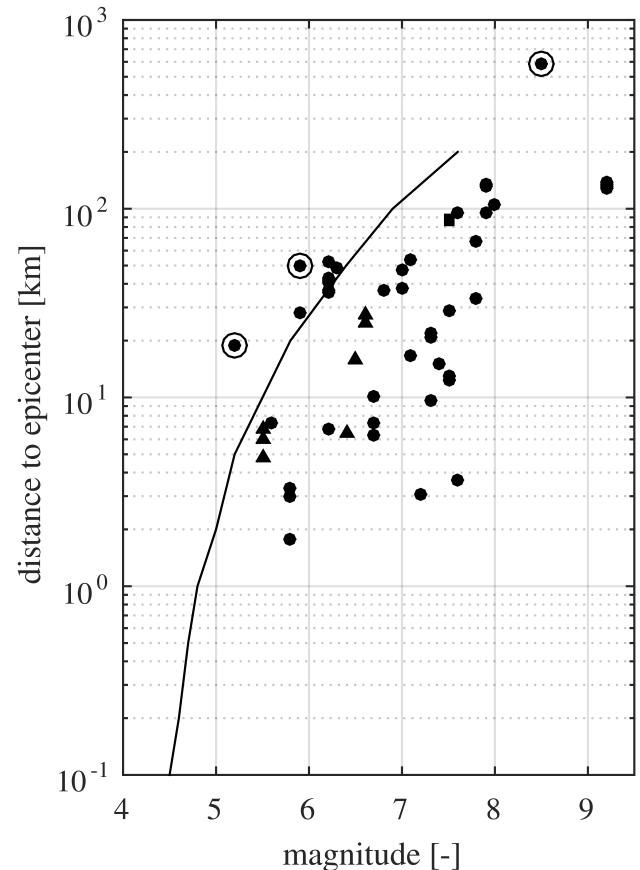
Fig. 4 - *Magnitude-distance relations of the 72 seismically induced landslides in the database caused by a specific earthquake. The curve represents the maximum distances from an epicenter at which coherent slides are to be expected according to KEEFER (1984) (dots for M_W, triangles for M_S, squares for M_{ukn}). Circled dots design the landslides of Laalam (M_W=5.2), Cerda (M_W=5.9) and Güevéjar (M_W=8.5)*

DATE	EARTHQUAKE	MAGNITUDE	LANDSLIDE	DISTANCE
21st of March 2006	Kherrata	M_W = 5.2	Laalam	19 km
6th of September 2002	Cerda (or Palermo)	M_W = 5.9	Cerda	50 km
1st of November 1755	Lisbon 1755	M_W = 8.5	Güevéjar I	578 km

Tab. 3 - *The three earthquake-triggered landslides significantly exceeding the reference curve (Fig. 4)*

Recurrence, completeness and distributions of assessed data

After completion of the data assessment raises the question about the data quality. Of particular interest are the recurrence of distinct parameters, the completeness of survey charts per dataset and the way values of parameters are distributed. The following sections describe each of the three qualitative and quantitative features separately.

Recurrence of parameters

The recurrence of a distinct parameter refers to the question of how many times it is reported when comparing all 277 survey charts. For instance, in 165 cases literature reports the landslide volume, and hence the respective recurrence value amounts to 60%.

The second page of the survey chart contains in total 66 parameters. However, three of them – d_E, d_{0-ab} and d_{E-ab} – are always 0 by definition (Tab. 2). Therefore the evaluation of parameter recurrence was carried out only for the other 63 parameters (Tab. 4).

Among them there are direct and indirect – or calculated – parameters. The first type is reported directly from literature or measured from maps and cross sections, whereas the indirect parameters are those calculated by equations (Tab. 2). Parameters of the second type thus create new values employing those of direct parameters under the condition that all necessary factors of the equation are available.

It is important to mention that: for the evaluation of the recurrence of parameters direct and indirect parameters were treated in the same way and no weighting was performed although one might argue that some parameters may be more suitable to describe landslides than others.

A special parameter is d_{E-bel}. It represents the only overlap between the group of indirect parameters and those that are always 0 since it is the difference between d_E and d_{E-ab}, both of which are 0 by definition. To keep the number of exceptions low, d_{E-bel} was nevertheless included in the set of 63 parameters. Its recurrence, though, is always 100%.

Broadly speaking, it appears that direct and indirect parameters related to the delineation of maps and LCS reach higher percentages. The fact that they are reported more frequently throughout literature reflects also the way of investigation and analysis of landslides. For many engineering-geological purposes a map and an LCS are sufficient since 2D approaches remain the most widespread in slope stability assessment nowadays.

In contrast, TCS parameters are very rare and this evidence cannot be explained by impossible calculation because all TCS parameters are direct. Unfortunately, precisely those TCS features would be necessary for an exact definition of the 3D lateral confinement of a landslide mass and accurate stability analyses.

The indirect parameter with most complexly interlinked factors is the calculated volume V_{equ} (Eq. 1) including D, W, L_h and H_{0E}. Due to the requirement that all factors must be available to calculate such an indirect parameter, one might hence expect the respective recurrence to be very low. Strikingly, its recurrence amounts to 74% which is very satisfactory. The recurrence of V_{lit}, reaches only 60%. When comparing volumes at cases were both V_{equ} and V_{lit} exist, it appears that the ratios V_{lit}/V_{equ} oscillate well around 1 and hence no particular difference in order of magnitude can be detected between the two volume types. Therefore, and because of its higher availability, V_{equ} is later used as a classification criterion for landslide magnitudes.

Completeness of survey charts

The completeness of a survey chart indicates the amount of available parameters. Likewise to the evaluation of the parameter recurrence, the reference number of parameters is 63 and an ideal case (where all parameters are available) would have a completeness of 100%.

Throughout the statistical analyses three datasets are defined of which two are in fact sub-sets:
• set "full": including all 277 landslides in the database;
• set "SR": including all 220 landslides in seismic regions;
• set "EQt": including all 99 landslides with a seismic trigger.

The set "full" incorporates both the set "SR" and the set

TYPE	R < 5%	30 ≤ R < 70%	R ≥ 70%
direct parameters	d_{1t}, d_{2t}, d_{3t}, γ_{1L}, γ_{2L}, γ_{3L}, γ_{1R}, γ_{2R}, γ_{3R}, rough width shapes (12)	V_{lit}, A, α_{lit}	principal geometry (1), H_{max}, H_{0E}, L_h, W, w_0, w_1, w_2, w_3, w_E, D, d_0, d_1, d_2, d_3, d_{1-ab}, d_{2-ab}, d_{3-ab}, δ_0, δ_1, δ_2, δ_3, δ_E
indirect parameters		A_h	V_{equ}, α_{equ}, D/L, w_{av}/L_h, H_{max}/L_h, L, l_{1-4}, l_{h1-h4}, w_{av}, d_{av}, d_{0-bel}, d_{1-bel}, d_{2-bel}, d_{3-bel}, d_{E-bel}

Tab. 4 - Recurrence (R) of the landslide parameters of page 2 of the survey chart (excluding d_E, d_{0-ab} and d_{E-ab} which are always 0 by definition)

"EQt", whereas the set "EQt" is only a part of the set "SR". Especially for numerical modeling of landslides undergoing seismic shaking, this separation is of particular importance allowing for comparison of the behavior of landslides in general, those being located in seismic regions and those having indeed a seismic trigger.

Figure 5 shows the completeness of survey charts for the three sets. It can be seen that within each set almost two thirds of the cases are complete to an extent of 50% to 70%. Also this result is very satisfactory since it testifies a high availability of parameters which in succession is required for the evaluation of the distributions of values of distinct parameters.

Combining the outcome of the evaluation of the parameter recurrence with the one of the survey chart completeness, it appears that a high completeness must be based on map- and LCS-related parameters. This reflects again the fact that obviously landslide studies are commonly limited to two dimensions, while full 3D representations which would allow for detailed 3D modeling are rather seldom.

Distributions of parameters

Another major feature of parameters is their statistical behavior in terms of value distribution. Unlike mentioned in the above sections of recurrence and completeness of data, distributions can only be evaluated for 49 of the geometrical parameters appearing on the second page of the survey charts due to the fact that some parameters do not register values. The rubric of principal geometry stores a word and the rubric on rough width shapes of the TCS contain a checkbox. Moreover, the parameters always being 0 (d_E, $d_{0\text{-}ab}$, $d_{E\text{-}ab}$ as well as the above mentioned

special case $d_{E\text{-bel}}$) are not included since their distributions would show only a zero line. For completeness, it is worth noting that the categories of the principal geometries are almost uniformly distributed within the database (32% rotational, 31% translational, 37% roto-translational).

Values for each individual parameter were grouped into histograms to fit different distribution curves on them in a second step. For all parameters histograms with 10, 30, 50 and 100 bins were computed, of which finally only the histograms with 30 bins were taken into consideration. It turned out that grouping to 10 bins results in a too coarse representation hindering accurate curve fitting, whereas 50 or 100 bins create a too detailed image making curve fitting difficult as well. By the means of Matlab's Curve Fitting Tool a normal (Eq. 2), a power law (Eq. 3) and an exponential (Eq. 4) distribution were fitted to each set of values per parameter. Best fits were chosen considering the coefficient of determination (R^2), the root mean square error (RMSE) and the best approximations of the coefficients a, b and c with 95% confidence bonds.

$$f(x) = a\, e^{-[(x-b)/c]^2} \qquad \text{(Eq. 2)}$$
$$f(x) = a\, x^b \qquad \text{(Eq. 3)}$$
$$f(x) = a\, e^{bx} \qquad \text{(Eq. 4)}$$

Applying this procedure to all 49 parameters for each of the three datasets ("full", "SR", "EQt"), two types of statistical distributions emerge as suitable to characterize the histograms. All values of dimension-related parameters manifest a clear decreasing exponential behavior, i.e. the histograms of 1D, 2D or 3D parameters show a progressively smaller number of occurrences with increasing parameter magnitude. – A very
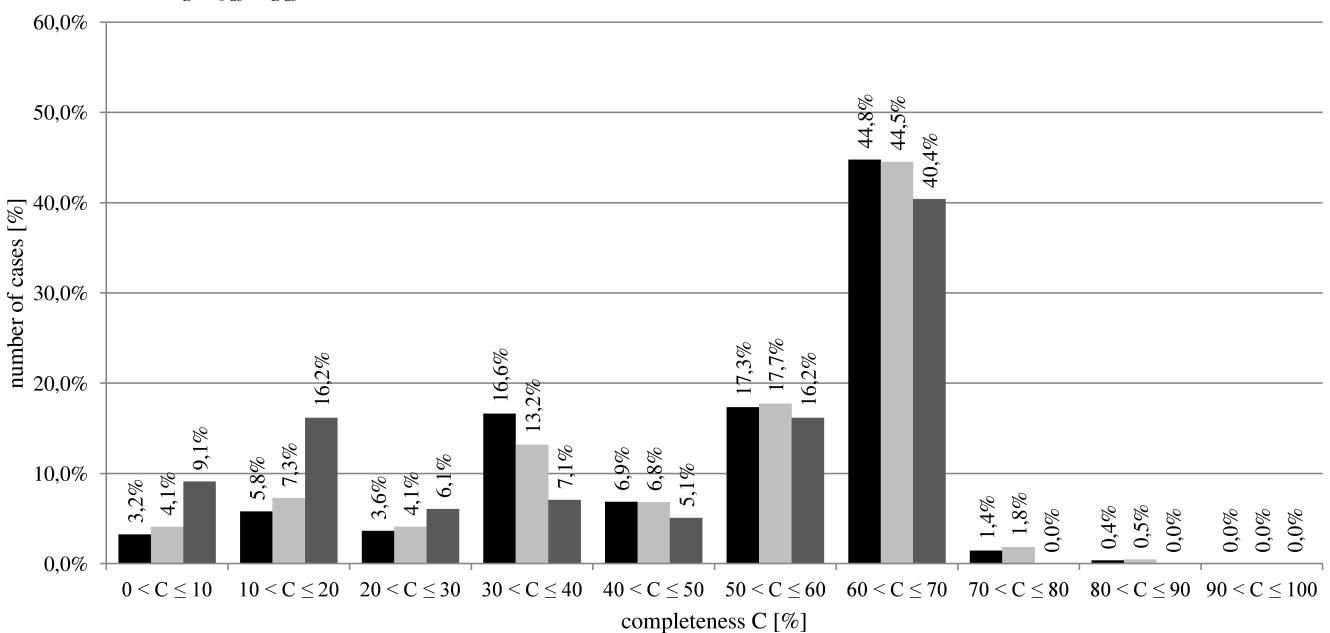

Fig. 5 - *Histograms showing the completeness (C) of the survey chart (set "full" in black, set "SR" in light grey, set "EQt" in dark grey)*

common phenomenon in nature and comparable for example to the Gutenberg-Richter-Law relating the total number of earthquakes having a magnitude larger than a given magnitude in a given region and time period (GUTENBERG & RICHTER, 1956). The "exponential family" hence includes lengths, widths, depths (excluding depth parts), heights, surfaces and volumes (Fig. 6).

By contrast, to all histograms of shape-related parameters normal distributions curves fit best; the angles along the rupture surface, the mean slope angle and the ratios form the "normal family" (Fig. 6). Curiously, also the depth parts belong to this family although they are 1D parameters. One possible explanation might be that the depth parts are by definition only parts of the entire depths at the five main positions of a landslide (Fig. 3). They are created by intersecting a depth with the line of the mean slope angle, and therefore it is not unreasonable to believe that they could bear traits of proportions and hence rather belong to the "normal family".

In the course of statistical analyses the question arose, if large landslides affect the division of parameters into the two families. For instance, it was unclear if exceptional high values of volume elongate the tail of a decreasing exponential distribution curve and if the distribution is only therefore classified as such. Thus a temporary reduction of the biggest landslides was performed, removing all cases with $V_{lit} > 10^9$ m³. Thereupon the procedure described above was carried out for the parameters L, A and V_{lit} of the dataset "full" to have a comparative histogram for a 1D, 2D and 3D parameter respectively. However, it turned out that the presence or absence of the biggest landslides in the histograms does not affect the results obtained by Matlab's Curve Fitting Tool and the distinction of families remains the same.

Mean geometries of landslides

Besides the consideration that dimension and shape of landslides might behave differently with increasing event size, there are also grounds for assumption that a landslide prototype could possibly be deduced from the database by averaging parameters and creating thereupon a mean geometry in the form of an LCS. Indeed, this is a promising approach for comparative studies because mean LCS can hence be derived not only for landslides in general (set "full"), for landslides in seismic regions (set "SR") or for seismically induced landslides (set "EQt"), but also for any other sub-set according to the desired filtering.

Averaging of parameters

Initially averaging of parameters was carried out for the three datasets separately, i.e. for each of the 49 parameters (cf. *Distributions of parameters*) the mean value was calculated regardless of how many times they were reported or calculated as indirect parameters (cf. *Recurrence of parameters*). It is important to mention that a mean value might thus be derived from a multitude of values or from only a few entries. Furthermore, mean values of different parameters are very likely to be derived from different pools of landslides since the completeness of the individual survey charts never reaches 100% (cf. *Completeness of survey charts*).

Unfortunately, this simple way of averaging did not show satisfactory results; most likely the landslide dimensions are by far too diverging to be represented by one single value per parameter. Proof for this assumption was provided by a simple multi-step test: 1) for all direct and indirect parameters mean values were calculated in Microsoft Access; 2) all "direct" mean values were inserted to a blank survey chart as if they represented values of a real case; 3) the survey chart automatically calculated from those "direct" mean values its own version of "indirect" mean values which at the end could be compared to the "indirect" mean values calculated initially by the Access database (Fig. 7). The differences between the two types of "indirect" mean values were more than obvious. Especially the mean values of A_h and V_{equ} appeared to be tremendously variable.

As simple averaging per dataset was apparently unsuitable for the definition of mean geometries, a more explicit distinction of
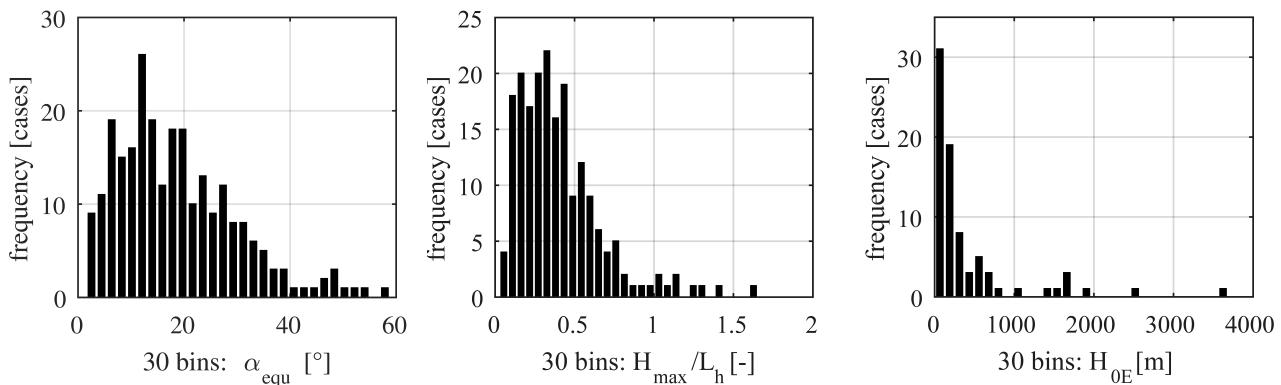
Fig. 6 - Examples of statistical distribution types. Histograms of angles as well as ratios were best fitted by normal distributions and are here exemplarily represented in a) by α_{equ} of the set "full" and in b) by H_{max}/L_h of the set "SR". Histograms of 1D, 2D and 3D parameters follow exponential distributions and are here exemplarily represented in c) by H_{0E} of the set "EQt"

the landslide dimension was necessary. Consequently landslides were grouped by order of magnitude (in decimal power) of their calculated volume V_{equ} (Fig. 8). This classification resulted in nine groups which were later united to three groups per dataset preserving the overall character of the statistical distribution. Attention has to be paid to the fact that due to the grouping process only landslides with existent records of V_{equ} could be taken into account, and therefore only those could contribute their parameters for the later averaging procedure.

The fact that V_{equ} became the parameter according to which groups were formed requests more precision. Although often difficult to measure, the volume of a landslide is its most significant parameter of characterization. It directly relates to the event magnitude and subsequently to the consequences it may cause (MALAMUD *et alii*, 2004). Thus, the grouping criterion was selected to be volume-based. Since the database theoretically reports V_{lit} and V_{equ} for every landslide – two occasionally quite different values – one of them had to be chosen. Among all 277 landslides in the database 165 report a V_{lit} and even though some of the landslides date back to times where DEMs were not as accurate as today no significant over- or under-estimations of
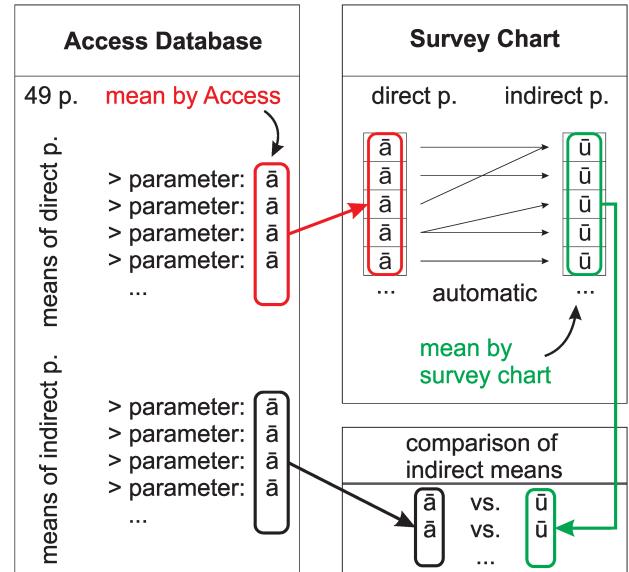
Fig. 7 - Illustration of the test procedure to compare mean values of indirect parameters calculated by the database and mean values of indirect parameters calculated by the survey chart
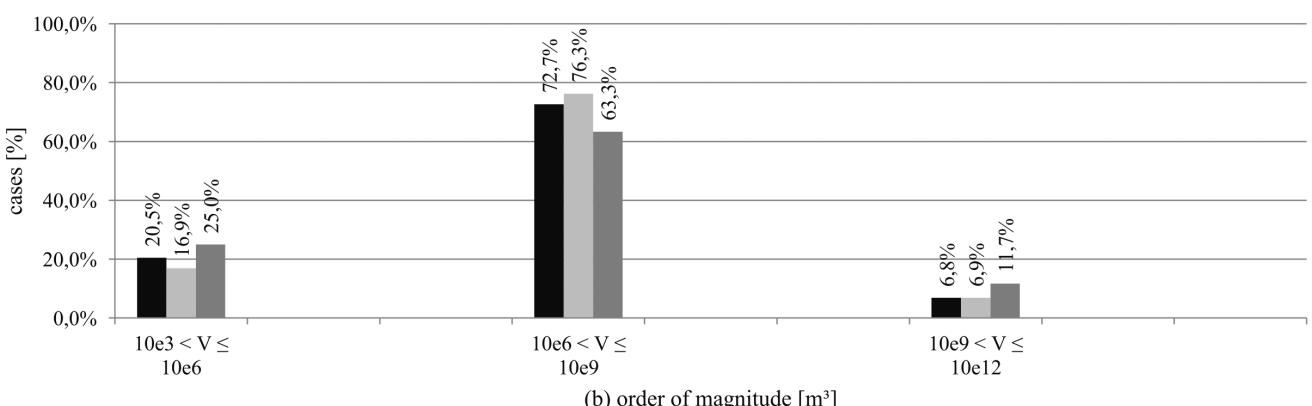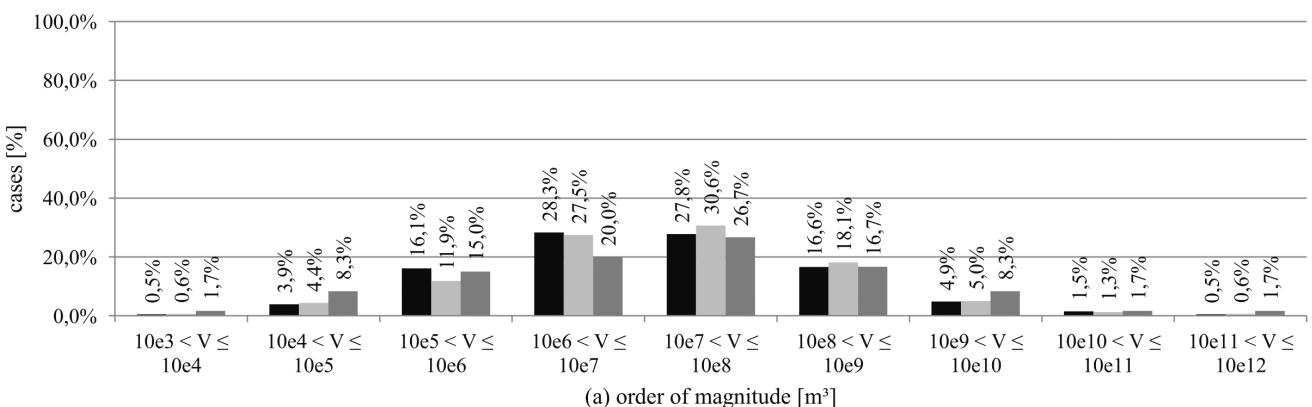
Fig. 8 - Number of landslides (in percent of the referring set) by order of magnitude of their calculated volume (V designing V_{equ}). The arrangement to 3 groups shown in b) preserves the statistical character of the distribution appearing in a)
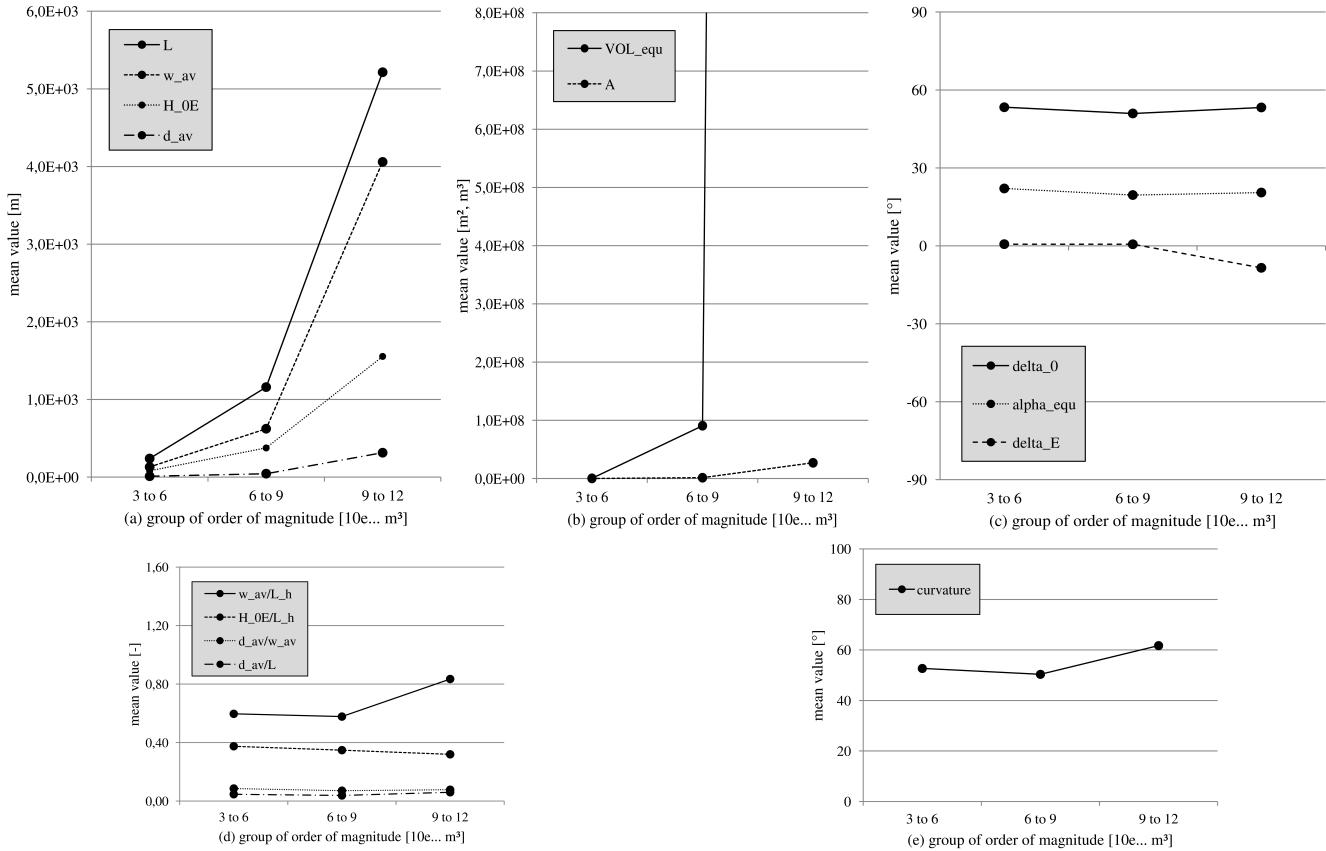
Fig. 9 - Development of mean values with increasing order of magnitude for the set "SR". Part a) shows the 1D parameters L, H_{0E}, w_{av}, d_{av}; part b) shows the 2D parameter A and the 3D parameter V_{equ}; part c) shows the shape-related parameters α_{equ}, δ_0, δ_E; part d) shows the four newly defined ratios d_{av}/L, d_{av}/w_{av}, w_{av}/L_h, H_{0E}/L_h and part e) shows the curvature

their volumes were found. On the contrary, 205 cases dispose of a V_{equ}. A strong argument against the choice of V_{equ} is the way of its calculation (Eq. 1); it is suitable for rotational landslides (CRUDEN & VARNES, 1996) while applying it to translational landslides it causes a volume loss and thus an underestimation of the actual volume. However, after comparing V_{lit} and V_{equ} at cases where both were available, differences appeared to be negligible and V_{equ} was adopted as the parameter according to which grouping should be performed.

With the new approach of grouping and averaging mean values along with their respective standard deviations were obtained for the 49 concerned parameters and for the three datasets. This time, the results appear to be very satisfying as shown by the before described test procedure (Fig. 7). "Indirect" mean values calculated by the survey charts came extremely close to the ones calculated by the Access database.

Representative for all 49 parameters, Fig. 9 shows the mean values for four 1D parameters (L, H_{0E}, w_{av}, d_{av}), the 2D parameter A, the 3D parameter V_{equ} as well as three shape-related parameters (α_{equ}, δ_0, δ_E) and four newly defined ratios (d_{av}/L, d_{av}/w_{av}, w_{av}/L_h,

H_{0E}/L_h). Also a value for the curvature was created, which is by definition δ_0-δ_E, and whose mean values are represented likewise.

When comparing the behavior of these mean values with increasing magnitude group, one discovers that the mean values of all dimension-related parameters increase as it could be expected for progressively bigger landslides. From 1D to 3D parameters the increase itself becomes more rapid and the standard deviation gaps become relatively larger. Surprisingly though, the mean values of all shape-related parameters are remarkably constant throughout the different orders of magnitude.

The two findings apply without exception to all three datasets. Combining both of them, and at least on the basis of averaged landslides, one can conclude that with increasing magnitude of a landslide its dimension changes whereas its shape remains more or less the same.

An issue that deserves critical consideration is the inclusion of different mass movement types in the database and the question if "hiding" mass movements other than proper landslides could affect the statistical analyses. Ideally and based on the classification of VARNES (1978), only landslides composed of soil,

rock and/or debris are appropriate to be included in the database. Unfortunately it is not seldom that authors use terms describing mass movements in a very vague sense and cases that are described in one publication as a landslide might appear for instance as an earth flow elsewhere. Gradual transitions between mass movement types support misleading nomenclature even more.

This discrepancy appears 37 times within the database; 33 cases can also be seen as a deep-seated gravitational slope deformation (DSGSD) and four cases might also be considered as earth flows. For each of them, literature indicated a clear surface of rupture separating the moving mass from the underlying bedding. – A fact, that favors – but does not justify – the interpretation as a landslide mass and hence the inclusion in the database.

Compared to landslides, earth flows as well as DSGSD – though to a lesser extent – are clearly different especially in terms of shapes. Their presence in the database must therefore be regarded with caution and two tests were carried out to estimate their statistical influence. First, plotting V_{equ} over the sequential numbers attributed to the individual cases, it turns out at all three datasets that calculated volumes of the DSGSD and the earth flows are by far not the greatest; the respective data points mix well among the ones of landslides. Second, based on the full dataset only and without subdivision into groups of order of magnitude, a mean value study similar to the above described procedure was conducted. This allowed for comparison of mean values obtained by the filtering options listed in Tab. 5. For DSGSD alone higher mean values of L, H_{0E} and thus of H_{0E}/L_h stand out and also δ_0 and the curvature are higher; the mean values for the earth flows depict lower mean values of δ_0 and the curvature as well as a higher L but lower w_{av} and thus a lower w_{av}/L_h. Both findings are in good agreement with typical DSGSD and earth flow masses. Differences to a characteristic landslide mass are therefore obvious.

Nevertheless DSGSD and earth flows do not exceed landslides neither in terms of number nor of volume and it is unlikely that they influence the outcome of statistical analyses. Moreover, some of them might even be classified as landslide emphasizing this conclusion. In this case, "hiding" mass movements other than landslides are of lower importance to the overall outcome of analyzes. Though, the issue underlines the necessity of proper mass movement classification in literature in order to avoid misinterpretations.

Mean geometries

The mean values per parameter can be used to draw averaged LCS. By combination of the three datasets and the three groups of orders of magnitude one obtains nine LCS which are called "mean geometries" for simplicity (Fig. 10).

As predicted by the mean value study, it can be seen that the dimension changes with increasing order of magnitude, but the shapes of the mean geometries are very similar throughout all magnitude groups. Only a slight increase of convexity becomes

FILTERING	MEANING	CASES
LS	landslides only	240
LS & DSGSD	landslides with DSGSD only	273
LS & EF	landslides with earth flows only	244
LS & DSGSD & EF	corresponding to the dataset "full"	277
DSGSD	DSGSD only	33
EF	earth flows only	4

Tab. 5 - Numbers of cases obtained by filtering and combination of different mass movement types

apparent at bigger orders of magnitudes, which is probably an effect related to emerging topography. Naturally topography is more relevant at landslides with a length of several kilometers than at those being only several meters long. With respect to dimensions, the three smallest mean geometries stand out inasmuch as the LCS of the set "SR" is about 50 m longer and the LCS of the set "EQt" about 30 m shorter in comparison to the one of the set "full". This evidence might seem significant at the first sight, but becomes negligible when considering length differences of up to around 100 m at the mean geometries of the intermediate magnitude group and of several hundreds of meters at those of the biggest magnitude group.

Furthermore, the shape does not change for different datasets; i.e. the mean geometry of all landslides does not differ from neither the one of the landslides in seismic regions nor the one of the seismically induced landslides.

CONCLUSIONS

A chronological database of landslides with various triggers was built. It contains 277 globally distributed cases of which one third has a seismic trigger. The term landslide refers to proper sliding mechanisms as defined by VARNES (1978).

By means of survey charts every landslide was comprehensively assessed giving general information such as location, date, triggering factors, material, sliding mechanism, event chronology, consequences and related literature on the one hand, and on the other hand information with respect to the landslide mass. The survey chart assured the maintenance of predefined standards during the acquisition process and it kept the bias as low as possible. The thereon appearing geometrical parameters are a further and more detailed development of the parameter set proposed by the INTERNATIONAL GEOTECHNICAL SOCIETIES' UNESCO WORKING PARTY ON WORLD LANDSLIDE INVENTORY (1990, 1991, 1993, 1994) and the INTERNATIONAL UNION OF GEOLOGICAL SCIENCES WORKING GROUP ON LANDSLIDES (1995). The entire content of all survey charts was introduced to a Microsoft Access database which now serves as a query tool to explore the data; it allows not only for data storing, but also for fast and efficient filtering, sorting and data preparation for statistical analyses of 2D and 3D landslide geometries.

Several statistical analyses were carried out to test the database itself in terms of qualitative and quantitative features, and
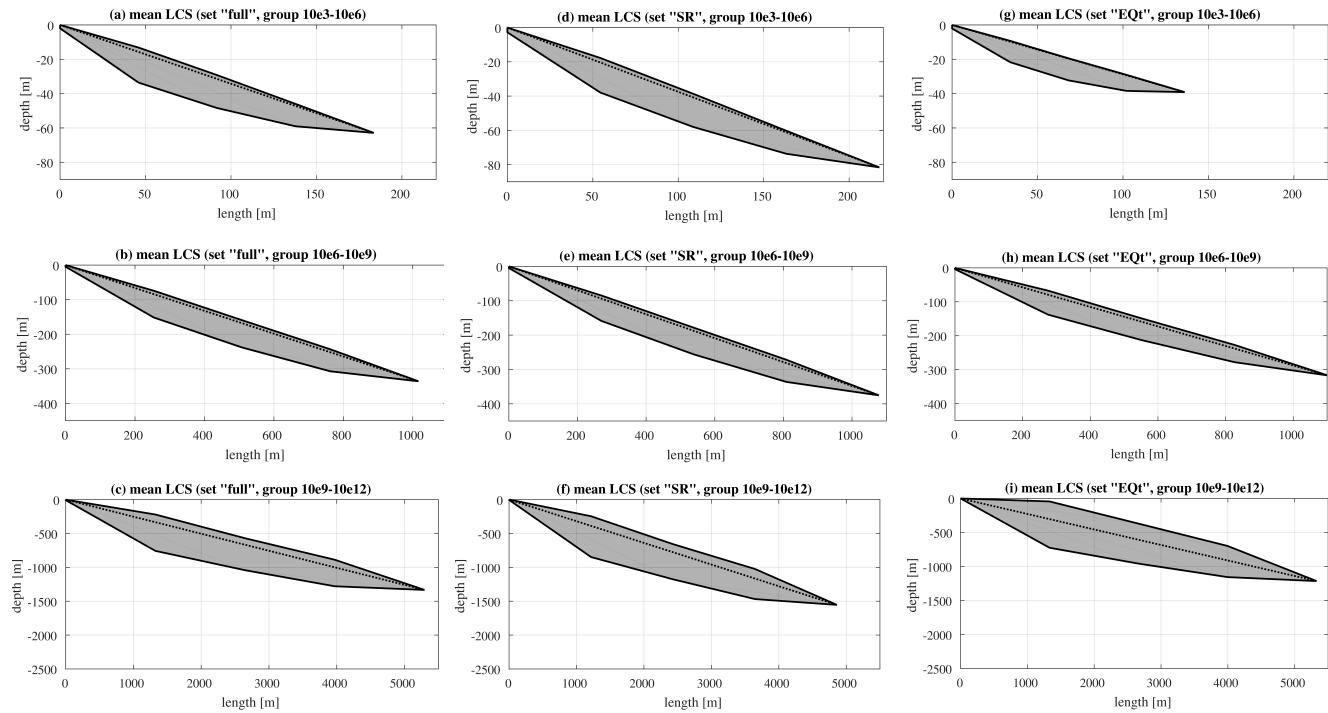
Fig. 10 - *Mean geometries of landslide masses confined by topographic surface and surface of rupture. The dotted line indicates the mean slope angle and corresponds to the "line" (Fig. 3). The first column with the cross sections a), b) and c) refers to the set "full", the second column with the cross sections d), e) and f) refers to the set "SR" and the third column with the cross sections g), h) and i) refers to the set "EQt". The uppermost row is based on the smallest volume group (10^3-10^6 m³), the middle row on the medium volume group (10^6-10^9 m³) and the lowest row on the biggest volume group (10^9-10^{12} m³). For completeness it should be mentioned that c) shows the only LCS without a trench (i.e. d_0 and thus d_{0-bel} are not 0; Fig. 3)*

to evaluate the data it contains. According to the type of analysis, the dataset of interest might either be the totality of all landslides (set "full" with 277 cases), the sub-set of all landslides in seismic regions (set "SR", 220 cases) or the sub-set of all seismically induced landslides (set "EQt", 99 cases).

In a first step epicenter-to-landslide distances of cases included in the database were compared to maximum epicenter-to-landslide distances proposed by KEEFER (1984) for coherent slides. Data from the database appeared to fit very well to the proposed limits at different magnitudes, and even though the scatter is not to be neglected only 3 landslides clearly exceed the limit curve. Thus, the data of the database is in very good accordance with KEEFER's (1984) proposition, which is highly satisfactory since the landslides in the database are randomly assessed on a global basis.

The recurrence of distinct parameters in the database, i.e. the number of times the same geometrical parameter stores a value comparing all 277 survey charts, reveals that parameters related to the characterization of maps and LCS are more frequently assessed, whereas parameters related to TCS are very rare to show values. This result is promising for 2D modeling, but limits accurate 3D modeling due to the lack of information about the lateral confinement – and hence about the impedance

contrast – of a landslide mass which is of particular interest when studying the soil response under seismic shaking. Strikingly, the calculated volume V_{equ} – even though being a parameter depending on many others – shows a very high recurrence. This emphasizes the choice of V_{equ} to be the parameter according to which landslides are grouped for further analysis.

The completeness of survey charts, i.e. the number of parameters storing a value per survey chart, shows that two thirds of all survey charts are complete to an extent of 50-70%. Roughly the same percentages are obtained for the three sets of interest which is again promising for 2D but less satisfactory for 3D modeling because full completeness is apparently not achieved at the expense of missing TCS information.

The combining of the results from the recurrence and the completeness studies, and the fact that the choice of landslides and their associated literature was random, reflects also the quality of landslide assessment in general. If more attention was paid to the widthwise characterization of a landslide, 3D models could be much more precise.

Later, values per parameter were grouped in histograms with 30 bins each to fit a normal, a power or an exponential distribution to them. Surely it is not ideal to fit distribution curves to histograms instead of ungrouped data, but unfortunately the values of a

particular parameter have no dependency on the sequential numbers. Testing all parameters in the three sets, histograms of dimension-related parameters manifest an exponential decrease whereas histograms of shape-related parameters were best fitted by normal distributions. The presence or absence of extremely large landslides did not affect the outcome.

The main request to the database was to delineate geometries that represent averaged shapes of rupture masses of landslides. After it turned out that averaging values of distinct parameters on the basis of whole sets is not suitable because of far too big and thus incomparable dimensions, a more explicit distinction was made. Landslides per set were united according to their calculated volume Vequ into three groups of the following orders of magnitude: $10^3 < V_{equ} \leq 10^6$, $10^6 < V_{equ} \leq 10^9$ and $10^9 < V_{equ} \leq 10^{12}$ in m³. The result of this grouping (Fig. 7) revealed a significant surplus of cases in the middle class leaving the question open if this distribution is globally representative implying a roll-over, or if – by chance – it is caused by the choice of landslides included in the database. The latter explanation remains arguable since the number of cases is high and no strategy was followed during the data assessment.

The grouping approach resulted in nine series of mean values of distinct parameters by combination of 3 sets and 3 classes of order of magnitude. Comparison of mean value behavior with increasing order of magnitude confirmed a different behavior of dimension- and shape-related parameters. Mean values of 1D, 2D and 3D parameters increase progressively with bigger orders of magnitude, whereas mean values of angles, ratios and the curvature remain rather constant. Using those mean values finally nine mean LCS in 2D (Fig. 10) were delineated which illustrate well the three major findings of the entire study:

- statistically, dimensions and shapes do not behave in the same way with increasing order of magnitude
- the shape is rather independent of the dataset
- the shape is slightly dependent on the order of magnitude

The three facts are of particular importance to numerical modeling and the evaluation of seismically induced displacements of soils undergoing external loads, since the shape of a landslide mass governs the seismic interaction with the underlying bedrock, but the dimension controls the intensity of the expected seismic effects including induced displacements (Lenti & Martino, 2013). The different mean geometries serve hence as landslide prototypes of varying dimensions to explore differences between 2D and 3D models having the same framework conditions (geometry, material, etc.). On the basis of these examples, it will be possible to compare displacements predicted by traditional slope stability methods such as the Newmark Sliding Block Method (Newmark, 1965) and results from numerical methods considering characteristic periods T_l/T_m and T_s/T_m linked to longitudinal and vertical dimensions of a system. At this context, Lenti & Martino (2013) describe systematic under- and over-estimations of displacements obtained by Newmark's (1965) method in comparison to results from numerical modeling. They also point out that horizontal displacements strongly depend on characteristic periods.

To conclude, it should be noted that, first, landslides are complex phenomena and averaged shapes of appearance like the ones presented in this study might serve for general research but cannot be used as representatives for the investigation of a particular site. Second, the statistical procedure presented in this article describes only one approach of evaluation with a specific focus of interest. Many other analyses may be conducted upon this vast and newly updated database and the creation of new input data for studies with different purposes is possible at any time.

ACKNOWLEDGEMENTS

DATA SOURCES

Data included in the database does not belong to the authors of this article. The following references do not include publications associated to the individual landslides (cf. Appendix I). However, it is possible at any time to provide a full list of evaluated literature for every case.

REFERENCES

Ambraseys N.N. & Bilham R. (2012) - *The Sarez-Pamir earthquake and landslide of 18 February 1911.* Seismological Research Letters, **83**: 294-314.

Bird J.F. & Bommer J.J. (2004) - *Earthquake losses due to ground failure.* Engineering Geology, **75**: 147-179.

Bozzano F., Lenti L., Martino S., Montagna A. & Paciello A. (2011) - *Earthquake triggering in highly jointed rock masses: reconstruction of the 1783 Scilla rock avalanche (Italy).* Geomorphology, **129**: 294-308.

Carson M.A. & Kirby M.J. (1972) - *Hillslope form and process.* Cambridge Geographical Studies No. 3, viii+475, Cambridge University Press, New York, United States of America.

Commission on Landslides of the International Association of Engineering Geology (1990) - *Suggested nomenclature for landslides.* Bulletin of the International Association of Engineering Geology, **41**: 13-16.

CRUDEN D.M. & VARNES D.J. (1996) - *Landslide types and processes.* In: TURNER A.K. & SCHUSTER R.L. (1996, EDS.). - *Landslides: investigation and mitigation.* Transportation Research Board, Special Report 247, 36-75, National Academy Press, Washington D. C., United States of America.

DUNNING S.A., MITCHELL W.A., ROSSER N.J. & PETLEY D.N. (2007) - *The Hattian Bala rock avalanche and associated landslides triggered by the Kashmir Earthquake of 8 October 2005.* Engineering Geology, **93**: 130-144.

EUROPEAN ARCHIVE OF HISTORICAL EARTHQUAKE DATA (2016) - *Catalog of the European archive of historical earthquake data.* Data retrieved from: http://www.emidius.eu/AHEAD.

EVANS S.G. & BENT A.L. (2004) - *The Las Colinas landslide, Santa Tecla: a highly destructive flowslide triggered by the January 13, 2001, El Salvador earthquake.* Geological Society of America Special Papers, **375**: 25-38.

GUZZETTI F., ARDIZZONE F., CARDINALI M., ROSSI M. & VALIGI D. (2009) - *Landslide volumes and landslide mobilization rates in Umbria, central Italy.* Earth and Planetary Science Letters, **279**: 222-229.

GUTENBERG B. & RICHTER C.F. (1956) - *Magnitude and energy of earthquakes.* Annals of Geophysics, **9**: 1-15.

INTERNATIONAL GEOTECHNICAL SOCIETIES' UNESCO WORKING PARTY ON WORLD LANDSLIDE INVENTORY (1990) - *A suggested method for reporting a landslide.* Bulletin of the International Association of Engineering Geology, **41**: 5-12.

INTERNATIONAL GEOTECHNICAL SOCIETIES' UNESCO WORKING PARTY ON WORLD LANDSLIDE INVENTORY (1991) - *A suggested method for a landslide summary.* Bulletin of the International Association of Engineering Geology, **43**: 101-110.

INTERNATIONAL GEOTECHNICAL SOCIETIES' UNESCO WORKING PARTY ON WORLD LANDSLIDE INVENTORY (1993) - *A suggested method for describing the activity of a landslide.* Bulletin of the International Association of Engineering Geology, **47**: 53-57.

INTERNATIONAL GEOTECHNICAL SOCIETIES' UNESCO WORKING PARTY ON WORLD LANDSLIDE INVENTORY (1994) - *A suggested method for reporting landslide causes.* Bulletin of the International Association of Engineering Geology, **50**: 71-74.

INTERNATIONAL SEISMOLOGICAL CENTER (2016) - *Bulletin of the International Seismological Centre.* Data retrieved from http://www.isc.ac.uk/iscbulletin.

INTERNATIONAL UNION OF GEOLOGICAL SCIENCES WORKING GROUP ON LANDSLIDES (1995) - A suggested method for describing the rate of movement of a landslide. Bulletin of the International Association of Engineering Geology, **52**: 75-78.

KEEFER D.K. (1984) - *Landslides caused by earthquakes.* Geological Society of America Bulletin, **95**: 406-421.

KEEFER D.K. (1994) - *The importance of earthquake-induced landslides to long-term slope erosion and slope-failure hazards in seismically active regions.* Geomorphology, **10**: 265-284.

KUROIWA J., DEZAA E. & JEAN H. (1970) - *Investigations of the Peruvian earthquake of May 31, 1970.* Proceedings of the 5th World Conference on Earthquake Engineering, Rome, Italy, **1**: 447-457.

LENTI L. & MARTINO S. (2013) - *A parametric numerical study of the interaction between seismic waves and landslides for the evaluation of the susceptibility to seismically induced displacements.* Bulletin of the Seismological Society of America, **103**: 33-56.

LOMNITZ C. (1970) - *The Peru Earthquake of May 31, 1970.* Bulletin of the Seismological Society of America, **60**: 1413-1416.

MALAMUD B.D., TURCOTTE D.L., GUZZETTI F. & REICHENBACH P. (2004) - *Landslide inventories and their statistical properties.* Earth Surface Processes and Landforms, **29**: 687-711.

MARTINO S., PRESTININZI A. & ROMEO R.W. (2014). - *Earthquake-induced ground failures in Italy from a reviewed database.* Natural Hazards and Earth System Sciences, **14**: 799-814.

NEWMARK N.M. (1965) - *Effects of earthquakes on dams and embankments.* Géotechnique, **15**: 139-160.

PREOBRAZHENSKY J. (1920) - *The Usoi Landslide.* Materials on general and applied geology of the Geologic Committee, **14**: 21 pp. (in Russian)

RODRÍGUEZ C.E., BOMMER J.J. & CHANDLER R.J. (1999) - *Earthquake-induced landslides: 1980-1997.* Soil Dynamics and Earthquake Engineering, **18**: 325-346.

SCHUSTER R.L. & ALFORD D. (2004) - *Usoi landslide dam and lake Sarez, Pamir Mountains, Tajikistan.* Environmental and Engineering Geosciences, **10**: 151-168.

USGS (2004) - L*andslide types and processes.* USGS Fact Sheet, 2004-3072, 4 pp.

VARNES D.J. (1978) - *Slope movement types and processes.* In: SCHUSTER R.L. & KRIZEK R.J. (1996, EDS.) - Landslides - Analysis and control. Transportation Research Board, Special Report, **176**: 11-33, National Academy Press, Washington D.C.

XU C., XU X.W., SHEN L.L., YAO Q., TAN X.B., KANG W.J., MA S.Y., WU X.Y., CAI J.T., GAO M.X. & LI K. (2016) - *Optimized volume models of earthquake-triggered landslides.* Scientific Reports, **6**: 1-9.

YIN Y.P., WANG F.W. & SUN P. (2009) - *Landslide hazards triggered by the 2008 Wenchuan earthquake, Sichuan, China.* Landslides, **6**: 139-151.

APPENDIX
I - List of landslides

No.	Date*	Landslide	Country	Earthquake	Region	Trigger
001.00	2001-03-18	Diezma	Spain	-	current seis.	-
002.00	1949-07-10	Khait	Tajikistan	Khait	current seis.	confirmed
003.01	paleo	Leupegem Hill 1	Belgium	-	low / no seis.	-
003.02	paleo	Leupegem Hill 2	Belgium	-	low / no seis.	-
003.03	paleo	Leupegem Hill 3	Belgium	-	low / no seis.	-
003.04	paleo	Rotelenberg Hill 4	Belgium	-	low / no seis.	-
003.05	paleo	Rotelenberg Hill 5	Belgium	-	low / no seis.	-
003.06	paleo	Rotelenberg Hill 6	Belgium	-	low / no seis.	-
003.07	paleo	Rotelenberg Hill 7	Belgium	-	low / no seis.	-
003.08	paleo	Rotelenberg Hill 8	Belgium	-	low / no seis.	-
003.09	paleo	Rotelenberg Hill 9	Belgium	-	low / no seis.	-
003.10	paleo	Rotelenberg Hill 10	Belgium	-	low / no seis.	-
003.11	paleo	Rotelenberg Hill 11	Belgium	-	low / no seis.	-
003.12	paleo	Rotelenberg Hill 12	Belgium	-	low / no seis.	-
003.13	paleo	Rotelenberg Hill 13	Belgium	-	low / no seis.	-
004.00	?	Büyükçekmece	Turkey	-	current seis.	-
005.01	2008-05-12	Chengxi	China	Sichuan	current seis.	confirmed
005.02	2008-05-12	Xinbei Middle-School	China	Sichuan	current seis.	confirmed
005.03	2008-05-12	Tangjiashan	China	Sichuan	current seis.	confirmed
005.04	2008-05-12	Daguangbao	China	Sichuan	current seis.	confirmed
006.00	?	Lushan Hot Spring	Taiwan	-	current seis.	-
007.01	1969	Ain El Hammam	Algeria	-	current seis.	-
007.02	1970	Tigzirt City	Algeria	-	current seis.	-
007.03	2009	Tigzirt Port	Algeria	-	current seis.	-
007.04	1952	Azazga	Algeria	-	current seis.	-
008.00	2014-03-22	Oso-Steelhead	USA	-	current seis.	-
009.01	1811-12-16	Stewart	USA	New Madrid Seq. (#1)	current seis.	confirmed
009.02	1811-12-16	Campbell	USA	New Madrid Seq. (#1)	current seis.	confirmed
010.00	1981-03	Avignonet	France	-	current seis.	-
011.00	paleo	Braemore	New Zealand	-	current seis.	-
012.00	2001-01-13	Las Colinas	El Salvador	El Salvador	current seis.	confirmed
013.00	1994-01-08	La Salle en Beaumont	France	-	current seis.	-
014.00	1978	Harmalière	France	-	current seis.	-
015.00	1980-11-23	Calitri	Italy	Irpinia 1980	current seis.	confirmed
016.01	1999-09-20	Tsaoling	Taiwan	Chi Chi	current seis.	confirmed
016.02	1999-09-20	Jiufenershan	Taiwan	Chi Chi	current seis.	confirmed
016.03	1999-09-20	Hungcaiping	Taiwan	Chi Chi	current seis.	confirmed
017.00	2009-08-09	Shiaolin	Taiwan	-	current seis.	-
018.01	?	Lesachriegel	Austria	-	current seis.	-
018.02	?	Gradenbach	Austria	-	current seis.	-
019.00	1903-04-29	Frank	Canada	-	current seis.	-
020.01	1964-03-28	Potter Hill	USA	Alaska 1964	current seis.	confirmed
020.02	1964-03-28	Bluff Road	USA	Alaska 1964	current seis.	confirmed
020.03	1964-03-28	Turnagain Heights	USA	Alaska 1964	current seis.	confirmed
020.04	1964-03-28	Point Campbell	USA	Alaska 1964	current seis.	confirmed
020.05	1964-03-28	Point Woronzof	USA	Alaska 1964	current seis.	confirmed
020.06	1964-03-28	L Street	USA	Alaska 1964	current seis.	confirmed
020.07	1964-03-28	4th Avenue	USA	Alaska 1964	current seis.	confirmed
020.08	1964-03-28	Government Hill	USA	Alaska 1964	current seis.	confirmed
020.09	1964-03-28	Native Hospital	USA	Alaska 1964	current seis.	confirmed
021.00	1994-01-17	Calabasas	USA	Northridge	current seis.	confirmed
022.00	1999-08-17	Degirmendere (offshore)	Turkey	Izmit	current seis.	confirmed
023.01	?	Vaculov-Sedlo	Czech Republic	-	low / no seis.	-
023.02	?	Kobylska	Czech Republic	-	low / no seis.	-
023.03	?	Kopce	Czech Republic	-	low / no seis.	-
024.00	1980-05-18	Mt. Saint Helens	USA	with volcanic eruption	current seis.	confirmed
025.00	paleo	Lluta	Chile	-	current seis.	-
026.00	postglacial	Columbia Mountain	USA	-	current seis.	-
027.00	1990-06	Eureka River	Canada	-	low / no seis.	-
028.00	1939-04	Montagneuse River	Canada	-	low / no seis.	-
029.00	1959-05-19	Dunvegan	Canada	-	low / no seis.	-
030.01	2007-05-05	Fox Creek East	Canada	-	low / no seis.	-
030.02	2007-05-05	Fox Creek West	Canada	-	low / no seis.	-
031.01	1897	CN50.9	Canada	-	current seis.	-
031.02	1886	Goddart	Canada	-	current seis.	-
032.00	1883-10-12	Beaver Creek	Canada	-	low / no seis.	-
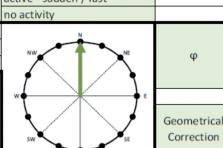
033.01	?	Mt. Cefalone	Italy	-	current seis.	-
033.02	?	Cima della Fossa	Italy	-	current seis.	-
033.03	?	Villavallelonga	Italy	-	current seis.	-
033.04	1915-01-13	Casali d'Aschi	Italy	Avezzano	current seis.	confirmed
033.05	1915-01-13	Gioia dei Marsi	Italy	Avezzano	current seis.	confirmed
033.06	1703-01-14	Mt. Alvagnano	Italy	Norcia 1703	current seis.	confirmed
033.07	?	Fiamignano	Italy	-	current seis.	-
033.08	?	Pescasseroli	Italy	-	current seis.	-
034.00	1780	Campo Vallemaggia	Switzerland	-	current seis.	-
035.01	?	Longobardi	Italy	-	current seis.	-
035.02	1982-12-13	Ancona	Italy	-	current seis.	-
036.00	1984-04	La Clapière	France	-	current seis.	-
037.00	2006-03-21	Laalam	Algeria	Kherrata	current seis.	confirmed
038.00	1806-09-02	Goldau	Switzerland	-	current seis.	-
039.01	1980	Cerentino	Switzerland	-	current seis.	-
039.02	1834	Peccia	Switzerland	-	current seis.	-
039.03	1846	Val Canaria	Switzerland	-	current seis.	-
039.04	1896-10	Val Colla	Switzerland	-	current seis.	-
040.01	1755-11-01	Güevéjar I	Spain	Lisbon 1755	current seis.	confirmed
040.02	1884-12-25	Güevéjar II	Spain	Arenas del Rey	current seis.	confirmed
041.00	1683	Montelparo	Italy	-	current seis.	-
042.00	1933-10	Sesa	Italy	-	current seis.	-
043.01	?	Ráztoka	Slovakia	-	low / no seis.	-
043.02	?	Polská Tomanová	Slovakia	-	low / no seis.	-
044.00	2002-10-31	Salcito	Slovakia	Molise 2002	current seis.	confirmed
045.01	paleo	Belbek	Ukraine	[name]	past seis.	uncertain
045.02	paleo	Frontovoye	Ukraine	[name]	past seis.	uncertain
045.03	paleo	Kacha 1	Ukraine	[name]	past seis.	uncertain
045.04	paleo	Kacha 2	Ukraine	[name]	past seis.	uncertain
045.05	paleo	Alma	Ukraine	[name]	past seis.	uncertain
045.06	paleo	Vishennoye	Ukraine	[name]	past seis.	uncertain
046.01	1692-09-18	Battice 1	Belgium	Verviers	current seis.	confirmed
046.02	1692-09-18	Battice 2	Belgium	Verviers	current seis.	confirmed
046.03	1692-09-18	Battice 3	Belgium	Verviers	current seis.	confirmed
046.04	1692-09-18	Battice 4	Belgium	Verviers	current seis.	confirmed
046.05	1692-09-18	Battice 5	Belgium	Verviers	current seis.	confirmed
046.06	1692-09-18	Battice 6	Belgium	Verviers	current seis.	confirmed
046.07	1692-09-18	Battice 7	Belgium	Verviers	current seis.	confirmed
046.08	1692-09-18	Battice 8	Belgium	Verviers	current seis.	confirmed
046.09	1692-09-18	Battice 9	Belgium	Verviers	current seis.	confirmed
046.10	1692-09-18	Battice 10	Belgium	Verviers	current seis.	confirmed
046.11	1692-09-18	Battice 11	Belgium	Verviers	current seis.	confirmed
046.12	1692-09-18	Battice 12	Belgium	Verviers	current seis.	confirmed
046.13	1692-09-18	Battice 13 (Manaihan)	Belgium	Verviers	current seis.	confirmed
047.01	2007-04-21	Acantilada Bay	Chile	Aysén	current seis.	confirmed
047.02	2007-04-21	Punta Cola	Chile	Aysén	current seis.	confirmed
047.03	2007-04-21	Mentirosa Island	Chile	Aysén	current seis.	confirmed
047.04	2007-04-21	Frío Creek	Chile	Aysén	current seis.	confirmed
047.05	2007-04-21	Marta River 1	Chile	Aysén	current seis.	confirmed
047.06	2007-04-21	Fernández Creek	Chile	Aysén	current seis.	confirmed
047.07	2007-04-21	Marta River 2	Chile	Aysén	current seis.	confirmed
047.08	2007-04-21	Pescado River	Chile	Aysén	current seis.	confirmed
048.00	1987-03-05	Salado	Ecuador	Ecuador	current seis.	confirmed
049.00	1679-06-04	Vokhchaberd	Armenia	Armenian 1679	current seis.	confirmed
050.00	1881-09-10	Castel Frentano	Italy	Lanciano	current seis.	confirmed
051.00	1997-10-11	Mt. Nuria	Italy	-	current seis.	-
052.01	1990-06-20	Galdian	Iran	Manjil-Rudbar	current seis.	confirmed
052.02	1990-06-20	Fatalak	Iran	Manjil-Rudbar	current seis.	confirmed
053.00	1963-10-09	Vajont	Italy	-	current seis.	-
054.00	2003-09-10	Tsaitichhu	Bhutan	-	current seis.	-
055.00	2007-03-01	S. Giovanni	Italy	-	current seis.	-
056.00	1950	Rasdeglia	Italy	-	current seis.	-
057.00	1992-08-19	Suusamyr	Kyrgyzstan	Suusamyr	current seis.	confirmed
058.01	paleo	Kokomeren	Kyrgyzstan	[name]	current seis.	uncertain
058.02	1885	Aksu	Kyrgyzstan	Belovodsk	current seis.	uncertain
058.03	paleo	Beshkiol	Kyrgyzstan	[name]	current seis.	uncertain
058.04	paleo	Karakudjur	Kyrgyzstan	[name]	current seis.	uncertain
058.05	1946	Sarychelek	Kyrgyzstan	Chatkal	current seis.	uncertain
058.06	paleo	Kugart	Kyrgyzstan	[name]	current seis.	uncertain
059.00	?	Rosone	Italy	-	current seis.	-
060.00	2000-04-09	Yigong	China	-	current seis.	-
061.00	1911-02-18	Usoi	Tajikistan	Sarez	current seis.	confirmed

062.01	1989-01-22	Okuli	Tajikistan	Gissar	current seis.	confirmed
062.02	1989-01-22	May 1	Tajikistan	Gissar	current seis.	confirmed
062.03	1989-01-22	Firma	Tajikistan	Gissar	current seis.	confirmed
062.04	1989-01-22	Sharara	Tajikistan	Gissar	current seis.	confirmed
063.00	1984	Klasgarten	Austria	-	current seis.	-
064.00	1975	Niedergallmigg	Austria	-	current seis.	-
065.01	1992	Huayuanyangjichang	China	-	current seis.	-
065.02	1996	Jinjinzi	China	-	current seis.	-
065.03	1999	Yangjiaba	China	-	current seis.	-
066.00	postglacial	Atemkopf	Austria	-	current seis.	-
067.00	2002-10	La Mania	Italy	-	current seis.	-
068.00	1960	Beauregard	Italy	-	current seis.	-
069.00	1965-01-09	Hope	Canada	[name]	current seis.	uncertain
070.00	?	Anlesi	China	-	current seis.	-
071.01	1914-05-30	Cà di Malta	Italy	-	current seis.	-
071.02	1934-03-06	Rocca Pitigliana	Italy	-	current seis.	-
072.00	1957-07-02	Kahrod	Iran	Mazandaran	current seis.	confirmed
073.00	2008-09	Cerca del Cielo	USA	-	current seis.	-
074.00	?	Kutlugün	Turkey	-	current seis.	-
075.00	1987-07-28	Val Pola	Italy	-	current seis.	-
076.01	?	Varco d'Izzo	Italy	-	current seis.	-
076.02	?	Costa della Gaveta	Italy	-	current seis.	-
077.00	1979-08-08	Abbotsford	New Zealand	-	current seis.	-
078.00	17th cent.	Tortum	Turkey	[name]	current seis.	uncertain
079.00	-300	Slumgullion	USA	-	current seis.	-
080.00	1999-05-13	Rufi	Switzerland	-	current seis.	-
081.00	2007	Zhujiadian	China	-	current seis.	-
082.00	1982	Minor Creek	USA	-	current seis.	-
083.00	2005-03-17	Kuzulu	Turkey	-	current seis.	-
084.00	1995	Huangtupo	China	-	current seis.	-
085.00	1998	Fosso Spineto	Italy	-	current seis.	-
086.00	-500000	Marcus	USA	-	current seis.	-
087.00	2003-11-09	Afternoon Creek	USA	-	current seis.	-
088.00	2009-04-26	Valgrisenche	Italy	-	current seis.	-
089.00	?	Aka-Kuzure	Japan	-	current seis.	-
090.00	?	Ivancich	Italy	-	current seis.	-
091.00	1999-11-12	Bakacak	Turkey	Düzce	current seis.	confirmed
092.00	postglacial	Triesenberg	Liechtenstein	-	current seis.	-
093.00	1783-02-06	Scilla	Italy	Calabria Seq. 2	current seis.	confirmed
094.00	1972	San Donato	Italy	-	current seis.	-
095.00	?	La Salsa	Italy	-	current seis.	-
096.00	1996	Grohovo	Croatia	-	current seis.	-
097.00	-35000	Uspenskoye	Russia	[name]	current seis.	uncertain
098.00	1995-01-16	Nikawa	Japan	Kobe	current seis.	confirmed
099.00	paleo	Dúdar	Spain	[name]	current seis.	uncertain
100.01	?	Machu Picchu A	Peru	-	current seis.	-
100.02	?	Machu Picchu B	Peru	-	current seis.	-
101.01	2002	Keillor Road	Canada	-	low / no seis.	-
101.02	1999-10-23	Whitemud Road	Canada	-	low / no seis.	-
102.00	1627-07-30	Vasto	Italy	Gargano	current seis.	uncertain
103.00	1963	Kostanjek	Croatia	-	current seis.	-
104.00	1997-07	Mt. Munday	Canada	-	current seis.	-
105.00	2010-08-06	Mt. Meager	Canada	-	current seis.	-
106.00	-10000	Downie	Canada	-	current seis.	-
107.00	2005-01-10	La Conchita	USA	-	current seis.	-
108.00	postglacial	Séchilienne	France	-	current seis.	-
109.00	2004	Ogoto	Japan	-	current seis.	-
110.00	2003	Kuchi-Otani	Japan	-	current seis.	-
111.00	1854-12-23	Zentoku	Japan	Tokai	current seis.	uncertain
112.00	2003-05-26	Tsukidate	Japan	Sanriku-Minami	current seis.	confirmed
113.01	1997-01	Slesse Park	Canada	-	current seis.	-
113.02	1973-05-26	Attachie	Canada	-	low / no seis.	-
114.00	1963-09-03	Lesueur	Canada	-	low / no seis.	-
115.00	1933-07	Brazeau	Canada	-	current seis.	-
116.00	1990-06-17	Saddle River	Canada	-	low / no seis.	-
117.00	2010-01	Cenes de la Vega	Spain	-	current seis.	-
118.00	1993-12-29	Acquara-Vadoncello	Italy	-	current seis.	-
119.00	1901-10-01	Boscobel	Barbados	-	current seis.	-
120.00	paleo	Mt. Nuovo	Italy	-	current seis.	-
121.00	-140000	Baga Bogd	Mongolia	-	past seis.	-
122.00	1974-04-25	Mayunmarca	Peru	-	current seis.	-
123.00	1612	Corniglio	Italy	-	current seis.	-

124.00	?	Vallcebre	Spain	-	current seis.	-
125.00	-10000	Corvara	Italy	-	current seis.	-
126.00	1786-06-01	Dadu River	China	Kangding-Luding	current seis.	confirmed
127.00	-10000	Fogo	Cabo Verde	with volcanic eruption	current seis.	confirmed
128.00	1906	Petacciato	Italy	-	current seis.	-
129.01	-20000	El Petruso	Spain	-	current seis.	-
129.02	-20000	Sextas	Spain	-	current seis.	-
129.03	-20000	La Selva	Spain	-	current seis.	-
130.00	1996	Halden Creek	Canada	-	low / no seis.	-
131.00	-10000	Åknes	Norway	-	low / no seis.	-
132.00	-10000	Kykula	Slovakia	-	low / no seis.	-
133.00	paleo	Latagualla	Chile	[name]	current seis.	uncertain
134.00	1920-12-16	Huihuichuan	China	Gansu	current seis.	confirmed
135.00	1980	Amloke Nakka	Pakistan	-	current seis.	-
136.00	1960-10	Tessina	Italy	-	current seis.	-
137.00	paleo	Krynica	Poland	-	low / no seis.	-
138.00	paleo	Collinabos	Belgium	-	low / no seis.	-
139.00	2002-09-06	Cerda	Italy	Cerda	current seis.	confirmed
140.00	2011-09-16	Shibangou	China	-	current seis.	-
141.00	1996-04-28	Quesnel Forks	Canada	-	current seis.	-
142.00	?	Riou-Bourdoux Valley	France	-	current seis.	-
143.00	2000-11-18	Slano Blato	Slovenia	-	current seis.	-
144.00	1958-07-10	Lituya Bay	USA	Alaska 1958	current seis.	confirmed
145.00	1976-05-06	Mt. Boscatz	Italy	Friuli 1976	current seis.	confirmed
146.00	1949	Kualiangzi	China	-	current seis.	-
147.00	-1500	Ropice	Czech Republic	-	low / no seis.	-
148.00	1982	La Valette	France	-	current seis.	-
149.00	postglacial	Heather Hill	Canada	-	current seis.	-
150.00	2008-11-23	Gongjiafang	China	-	current seis.	-
151.00	paleo	Utiku	New Zealand	-	current seis.	-
152.00	paleo	Taihape	New Zealand	-	current seis.	-
153.01	paleo	Stromboli	Italy	-	current seis.	-
153.02	paleo	La Fossa	Italy	-	current seis.	-
154.00	1909-11	East Lirio	Panama	-	current seis.	-
155.01	2010-11	Cischele	Italy	-	current seis.	-
155.02	?	Ochojno	Poland	-	low / no seis.	-
156.00	postglacial	Gammajunni 3	Norway	-	low / no seis.	-
157.00	postglacial	La Frasse	Switzerland	-	current seis.	-
158.00	1953-01-31	Miramar	United Kingdom	-	low / no seis.	-
159.00	?	Mahouane Dam	Algeria	-	current seis.	-
160.00	paleo	Pianello	Italy	-	current seis.	-
161.00	2011	Santa Maria Maddalena	Italy	-	current seis.	-
162.00	?	Zhaoshuling	China	-	current seis.	-
163.00	?	Dúrcal	Spain	-	current seis.	-
164.00	1935	Aggenalm	Germany	-	low / no seis.	-
165.00	?	Huangshipan	China	-	current seis.	-
166.00	postglacial	Lake Wanaka	New Zealand	[name]	current seis.	uncertain
167.00	2015-02-02	Mofjellbekken	Norway	-	low / no seis.	-
168.00	?	Badu	China	-	current seis.	-
169.01	paleo	Number 1	China	-	current seis.	-
169.02	paleo	Number 2	China	-	current seis.	-
170.01	2005-12-10	Saint Barnabé	Canada	-	low / no seis.	-
170.02	2010-05-10	Saint Jude	Canada	-	low / no seis.	-
170.03	1994-04-21	Sainte Monique	Canada	-	low / no seis.	-
171.00	1970	Bird	New Zealand	-	current seis.	-
172.00	2013-12-03	Montescaglioso	Italy	-	current seis.	-
173.00	19th cent.	Spriana	Italy	-	current seis.	-
174.00	?	Piscopio I Tunnel	Italy	-	current seis.	-
175.00	?	La Saxe	Italy	-	current seis.	-
176.00	?	Erguxi	China	-	current seis.	-
177.01	1955-12-07	Hawkesbury	Canada	blast	low / no seis.	uncertain
177.02	1962-05-23	Toulnustouc	Canada	blast	low / no seis.	uncertain
177.03	1996-06-20	Finneidfjord (offshore)	Norway	blast	low / no seis.	uncertain
177.04	2009-03-13	Kattmarka	Norway	blast	low / no seis.	uncertain
177.05	2009-08-01	La Romaine	Canada	blast	low / no seis.	uncertain
178.01	1960	Bumper	Australia	-	low / no seis.	-
178.02	1960	Siphon Gully	Australia	-	low / no seis.	-

(*) either the time of major failure or the time since when sliding is reported (for active landsides)

II - Survey chart

LANDSLIDE ID

Name		MM Type	
Earthquake		MM ⇆ EQ	
Date (precise or other indication)			
Fatalities			
Damage			
Location (km, direct., city, country)			

Location (Google Earth)	latitude		Dynamics	active - constant / slow
	longitude			active - sudden / fast
	m.a.s.l.			no activity
Material Classification	soil		Sliding Direction	
	rock	wind direction	degrees	
	debris		FAUX	φ

Geometrical Correction

LANDSLIDE IMAGERY
(this section refers to all related papers*)

Map	LCS	3D	Photo

LANDSLIDE CAUSE

Earthquake			Other	Unknown
Magnitude	Time Lag	General Seismic Area	water	
			wind	
			else	
			suspicion	

NOTES

assumption for map			knickpoints	
assumption for LCS			XZ-scales	
location problem		LCS	rupture zone	
slope modification			pre-LS surface	
MM includes / became			self-placed	
other notes				

RELATED PAPERS* (MM, EQ, Region, etc.)
(this section contains names as they appear in the paper collection: Name A. B., Name A. B. or et al., year)

	availability

LANDSLIDE GEOMETRY

Principal Geometry	Volume		Ratios	
(3 options: rot, trans, rototrans)	according to literature		D/L	#DIV/0!
	according to equation (only if rotation.) $V = (1/6).\pi.L.D.W$	#DIV/0!	W_m/L_h	#DIV/0!
			H_{max}/L_h	#DIV/0!

Longitudinal Cross Section (LCS)

Length	L	#DIV/0!	slope angle α	according to literature			
	$l_1 = ... = l_4$	#DIV/0!		according to equation		$\alpha = atan(H_R/L_h)$	#DIV/0!
Depth	D		depth parts	above line	below line	angles along rupture surface	
	d_0		d_{0-ab} & d_{0-bel}	0	0	δ_0	
	d_1		d_{1-ab} & d_{1-bel}		0	δ_1	
	d_2		d_{2-ab} & d_{2-bel}		0	δ_2	
	d_3		d_{3-ab} & d_{3-bel}		0	δ_3	
	d_E	0	d_{E-ab} & d_{E-bel}	0	0	δ_E	
	d_{av}	0					
Height	H_{RE}						
	H_{max}						

$cos(\alpha) = L_h/L$ Area

A	
A_h	#DIV/0!

Map

Length	L_h	
	$l_{h1} = ... = l_{hM}$	0
Width	W	
	w_0	
	w_1	
	w_2	
	w_3	
	w_E	
	w_{av}	#DIV/0!

0	0,2	0,4	0,6	0,8	1
1					
0,8					
0,6					
0,4					
0,2					
0					

Transversal Cross Sections

Transversal Cross Section I (TCS I)		Transversal Cross Section II (TCS II)		Tr. Cross Section III (TCS III)	
Width	w_1	0	Width	w_2	0	Width	w_3	0
Depth	d_1	0	Depth	d_2	0	Depth	d_3	0
	d_{11}			d_{2l}			d_{3l}	
Flank Angles	γ_{1L}		Flank Angles	γ_{2L}		Flank Angles	γ_{3L}	
	γ_{1R}			γ_{2R}			γ_{3R}	
Rough	V	(	Rough	V	(		V	(
Width Shape	[	U	Width Shape	[	U		[	U